STEADY STATE STRESS IN A COATED INFINITE HALF-SPACE SUBJECTED TO A MOVING LOAD

THESIS

Jason M. Cruthirds, 1st Lieutenant, USAF

AFIT/GCS/ENC/05-01

DEPARTMENT OF THE AIR FORCE
AIR UNIVERSITY

AIR FORCE INSTITUTE OF TECHNOLOGY

Wright-Patterson Air Force Base, Ohio

AFIT/GCS/ENC/05-01

STEADY STATE STRESS IN A COATED INFINITE HALF-SPACE SUBJECTED TO A MOVING LOAD

THESIS

Presented to the Faculty

Department of Mathematics and Statistics

Graduate School of Engineering and Management

Air Force Institute of Technology

Air University

Air Education and Training Command

In Partial Fulfillment of the Requirements for the

Degree of Master of Science in Computer Systems

Jason M. Cruthirds, BS

1st Lieutenant, USAF

March 2005

AFIT/GCS/ENC/05-01

STEADY STATE STRESS IN A COATED INFINITE HALF-SPACE SUBJECTED TO A MOVING LOAD

Jason M. Cruthirds
1st Lieutenant, USAF

Approved:

//Signed//	11 March 2005
William P. Baker (Chairman)	date
//Signed//	11 March 2005
Anthony N. Palazotto (Member)	date
//Signed//	11 March 2005
Lawrence K. Chilton (Member)	date

Abstract

This research investigates the use of coatings to mitigate the stress distribution into an infinite half-space. High energy impact phenomenon at velocities exceeding the speed of sound is an important area of research to the Air Force Research Laboratory. Holloman Air Force Base's High Speed Test Track sustains significant damage due to this phenomenon. In this thesis, the track system and coating are modeled analytically with equations of motion in terms of linear displacements. Coating thickness and material properties of epoxy or polymer laminates are investigated to understand their affect on stress distribution in the rail. An analytic solution is used to verify the numerical solutions. It is found that due to the limitations in coating thickness of the track system, this property has no significant affect on the stress distribution. However, the shear modulus of the material is found to have a significant affect representing the possible onset of material failure through the consideration of the combined stress field at the coating-rail interface.

Acknowledgements

I would like to express my sincere appreciation to my thesis advisor, Dr. William Baker, not only for his technical guidance, but also his patience and understanding throughout the course of this thesis effort. I would like to recognize Dr. Anthony Palazotto for sharing his incredible bank of knowledge and for his continued faith in my research. I would also like to thank Dr. Lawrence Chilton for serving on my committee. Finally, I would be remiss if I did not extend my appreciation to Dr. Neal Glassman of the Air Force Office of Scientific Research for his continuing financial support for AFIT's research on the high speed test track.

Table of Contents

List of Figures

Page

List of Tables

STEADY STATE STRESS IN A COATED INFINITE HALF-SPACE SUBJECTED TO A MOVING LOAD

Chapter 1. Introduction

1.1 General Issue

High energy impact phenomenon at velocities exceeding the speed of sound is an important area of interest to the Air Force today. Specifically, the Air Force Research Laboratory's Holloman AFB High Speed Test Track (HHSTT) has a special interest in studying this phenomenon.

The HHSTT has a rocket sled attached to a rail by a slipper. The rocket sled is a moving vehicle used to obtain velocities of exceptional magnitude in order to test propulsion components of interest to the Air Force. On April 29, 2003, HHSTT's hypersonic upgrades allowed a Missile Defense Agency payload to set a world land speed record at Mach 8.5 (2.8 km/sec). The goal of the HHSTT is to operate up to Mach 10 (3 km/sec) in air (1:1-1).

During high speed impact tests, the rail, composed of 1080 steel, sustains significant damage from a phenomenon known as hypervelocity gouging. Since repairing the damage of the rail is such a great expense, the HHSTT and the Air Force Office of Scientific Research seek methods to mitigate gouging. One method currently used is to paint thin polymer coatings on the rail. However, very little is known about the affect of these coatings on the stresses in the steel rail that lead to gouging.

1.2 Research Objectives

This research investigates the use of coatings to mitigate stress wave propagation into a half-space by high energy created by a load moving parallel to the surface at

constant hypersonic velocities. Particularly, it addresses the issues of coating thickness and shear modulus and their affect on the stress distribution within the rail. Further, it examines variable material properties through the thickness of the coating to analyze the effectiveness of layering coatings. This is carried out through a steady state solution.

1.3 Scope

Although it is of primary concern to the HHSTT, this study does not focus on the gouging phenomenon directly. There are many factors that cause gouging. One of the primary factors of concern is the distribution of stress in the rail. This research investigates the development of stress in a coated half-space prior to the onset of hypervelocity gouging to determine coating properties that may mitigate gouging before the phenomenon occurs.

There are many ways to model Holloman's track system. This research takes an analytic approach to the problem. The rail is modeled mathematically as an elastic half-space with a thin elastic layer bound to the half-space for the coating. The rail is considered infinite in length due to its size relative to the slipper. Displacement equations are used to describe stress distribution in both the rail coating and the half-space (rail). Material properties of the coating region are varied to investigate the affect these properties have on the distribution of stress in the half-space.

In order to represent a complete problem description, one would have to consider the nonlinear wave equations that permit the development of shock waves. This is not considered in this research, but certain important parameters, thickness and stiffness, related to coatings may be characterized based upon a steady state solution. To make the problem linear and mathematically tractable, several additional assumptions are made.

First, the effect of friction is introduced through the shear stress at the top boundary of the coating. The materials for the rail and coating are assumed to be isotropic, homogeneous, and obey Hooke's law. Also, the distribution of stress is assumed uniform through the width of the rail. Thus, the system is only modeled in two dimensions under a plane strain assumption. In other words, this study assumes zero displacement through the width of the rail. Further, this thesis only allows for small displacements to take place and ignores the high energy concerns which implies

$\sum forces = mass \times accelration$.

Figure 1 gives the geometry of the system taking into account the assumptions made for the problem. Region I is the thin coating and region II is the rail. The length of the slipper is $2l$ and the thickness of the coating is h. The segment of the coating where the load is applied is from $-l$ to l. The arrow pointing in the negative y direction signifies the direction of the direct load. The arrows pointing in the positive x direction signifies the direction of the shear stress and the motion of the shoe traveling at speed c_s.

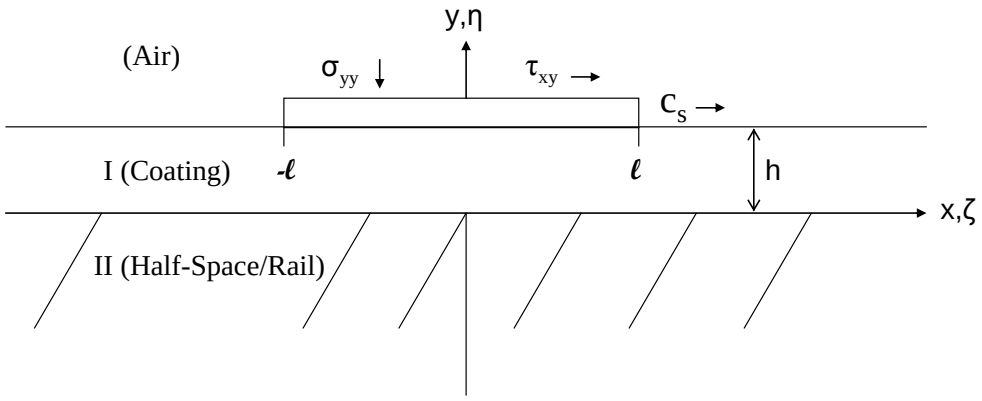

Figure 1. Geometry of the Coated Rail System

1.4 Literature Review

The transportation industry is the primary catalyst for research in half-space stress analysis. Many articles are published motivated by the study of highways and railways, with particular interests in soils and pavements. Although the focus of this research is not on soils and pavements, much of the theory, formulation, and techniques used to describe and solve the systems apply directly to this effort. This section outlines the ideas that have contributed to this research effort.

1.4.1 Beams

Beam-type structures are studied quite frequently with respect to half-spaces and moving loads. Lu Sun studied the dynamic response of a flexible beam resting on an elastic foundation (2). The governing equations are written in terms of small displacements and Green's functions are found using a spatial Fourier transform. Beam response is given in terms of convolutions with the Green's functions in accordance with linear operator theory. In another article, Sun studies Bernoulli-Euler beams resting on a viscoelastic foundation. The foundation is modeled as a Winkler foundation. Again Sun finds Green's functions and presents the analytic solution to the problem.

H.P. Lee studied the response of a beam with a moving source using the equations of motion for an Euler beam of fixed length (4). Lee nondimensionalized his parameters and used a Lagrangian approach to develop numerical results. Like Sun, Rao studied dynamic response of Bernoulli-Euler beams (5). Rao solved the dimensionless equations using a perturbation method, expanding modal coordinates in a series taking advantage of a small parameter in his study. Gbadeyan and Oni (6) and Choros and Adams (7) performed similar studies on beam-type structures.

1.4.2 Coatings

Soldatenkov discusses a thin elastic strip connected to an elastic half-space (8). He studied the effects of a disk-shaped load and formulated his problem in terms of wear and contact pressure. Soldatenkov uses the method of successive approximations to determine the wear in the strip. Aleksandrov and Arutiunian study two different types of coating, a thin fluid layer and a stiffener (9). Their equations are formulated in terms of mean displacement and tensile deformation and the boundary conditions are given in terms of stress. A Fourier transform is used to find solutions and asymptotic methods are used to determine approximate solutions. Finally, de Barros and Luco study the steady state response of a layered viscoelastic half-space to a moving point source in three dimensions (10). The moving load is characterized by the distribution of body forces per unit volume. The equations studied are formulated in terms of displacements and stresses. de Barros and Luco use Fourier analysis to find solutions and a Fast Fourier Transform to interpret the results in the spatial domain.

1.4.3 Equations of Motion

One thing that varies greatly from study to study is the equations used to solve the problems. Kennedy and Herrmann (11), Vigak (12), Dieterman and Metrikine (13) and Dal' (14) use Airy stress functions which are formulated in terms of displacement potentials. Some equations are used for very specific applications. Hu and Hartley formulate their problem in terms of plate deflection since they studied the separation between plates and half-spaces (15).

Verruijt and Cordova use the same form of the displacement equations as this

study (16). However, they model the half-space as a viscoelastic material rather than a pure elastic material. They formulate the boundary conditions in terms of stresses. Dimensionless parameters are determined to simplify the system and a moving coordinate system is introduced to ensure source of moving load is always at the origin. Fung solves a similar problem with a point source (17:258-269). His equations are solved in terms of displacement potentials. Fung's problem is not the same exact problem as this research, but his results are very similar and comparable.

1.5 Document Overview

Chapter 2 of this document examines the theory and equations governing the mechanics of the system. The equations of motion are introduced. Stress and strain are explained and used to determine appropriate boundary and initial conditions. Further, a coordinate transformation is used to produce a moving coordinate system and the equations of motion are scaled to create dimensionless parameters and variables. Finally, the steady state system is introduced.

Chapter 3 discusses the methods for setting up the system and the techniques for solving the problem. It starts with a discussion of the solutions to the problem if no coating were used. The analytic solution is found with no coating in the Fourier transform domain and the transform is inverted in terms of stresses. Since the problem with variable coating properties must be solved numerically, the analytic solution for the problem with no coating is presented in the transform domain but is primarily used to validate the finite difference method. The finite difference method is derived and compared to the analytic solution in the transform domain.

The fourth chapter starts with an analysis of the problem where the rail is directly

subjected to the moving load. A point source, a uniform distribution of applied force, and a parabolic distribution of applied force are used to study the behavior of stress in the rail. Then a comparison is made between applying the load directly to the rail and to a coated rail. The thickness and shear modulus are varied to determine their affect on the stress distribution in the rail. Finally, the shear modulus of the coating is varied as a function of thickness to examine the effects of layered coatings and a vanishing shear modulus at the top of the coating.

Chapter 5 provides a summary of this thesis. First the theory, methods, and solutions are reviewed. Then a synopsis of the behavior of stress in the rail with and without coating is presented along with the significant findings in this study. Finally, suggestions for future research are given.

Chapter 2. Theory and Governing Equations

2.1 Overview

This chapter discusses the general theory and presents the equations which model the stress distribution within the rail and the coating. First, the equations of motion are given which leads to a discussion on stress and strain expressed in terms of displacement. Then, stress waves are discussed as an important part of understanding the dynamics of the system. Next, the continuity, initial, and boundary conditions are determined. The equations of motion and the conditions are transformed through a coordinate transformation and scaled to give dimensionless equations of motion. Finally, the steady state equations are presented to simplify the problem.

2.2 Equations of Motion

The governing equations of motion will be expressed in terms of local displacements. That is, a particle at position (x, y) is displaced under loading to a position $(x+u(x,y,t), y+v(x,y,t))$ as illustrated in Figure 2.

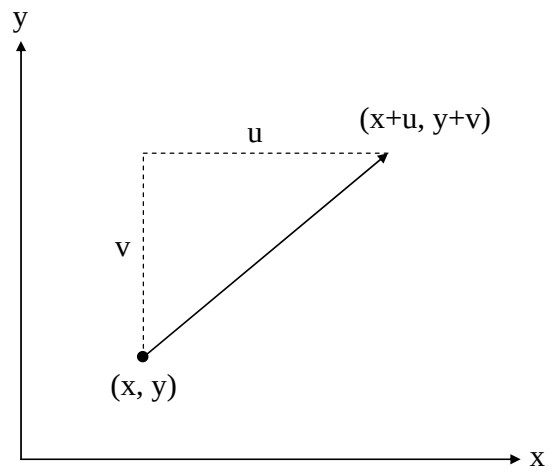

Figure 2. Example of Particle Displacement in Terms of Local Displacements

The functions u and v are used to construct the system of differential equations that describe the behavior of particles in the coating (region I) and the rail (region II) (18:486) (See Figure 1). Under the assumption of plane strain, the equations for the coating (region I) are

$$G_1 g(y)\Delta u_1 + \frac{G_1 g(y)}{1-2\upsilon_1}\frac{\partial e_1}{\partial x} = \rho_1 \frac{\partial^2 u_1}{\partial t^2} \qquad 2.2.1$$

$$G_1 g(y)\Delta v_1 + \frac{G_1 g(y)}{1-2\upsilon_1}\frac{\partial e_1}{\partial y} = \rho_1 \frac{\partial^2 v_1}{\partial t^2} \qquad 2.2.2$$

and inside the rail (region II) are

$$G_2 \Delta u_2 + \frac{G_2}{1-2\upsilon_2}\frac{\partial e_2}{\partial x} = \rho_2 \frac{\partial^2 u_2}{\partial t^2} \qquad 2.2.3$$

$$G_2 \Delta v_2 + \frac{G_2}{1-2\upsilon_2}\frac{\partial e_2}{\partial y} = \rho_2 \frac{\partial^2 v_2}{\partial t^2} \qquad 2.2.4$$

with

$$e_k = \frac{\partial u_k}{\partial x} + \frac{\partial v_k}{\partial y}; \quad k = 1, 2 \qquad 2.2.5$$

$$-\infty < x < \infty, \; y < 0, \; t > 0$$

where G is the modulus of elasticity in shear, ρ is the density, υ is Poisson's ratio for the material, and the subscript, k, is used to designate the region. The symbol Δ is the Laplacian operator such that $\Delta u = \frac{\partial^2 u}{\partial x^2} + \frac{\partial^2 u}{\partial y^2}$. The function $g(y)$ is introduced to account for variation in the shear modulus through the thickness of the coating and can vary from zero to one.

2.3 Stress and Strain

Stress is the force per unit area as a result of application of a load and can be expressed in two components, direct and shear. The direct stress at a point is the component acting normal to any plane perpendicular to the reference axis while the shear stress is acting parallel to that plane. This document uses σ_{ii} and τ_{ij} to denote direct and shear stress, respectively, where i is the reference axis and j is the direction of the stress component. Figure 3 shows the components of stress due to an applied force on a two-dimensional reference cell. The arrow labeled σ_{xx} is parallel to the x axis and signifies the direct stress perpendicular to the y-z plane while the arrow designated τ_{xy} is a shear stress and acts parallel to the y-z plane in the direction of the y axis.

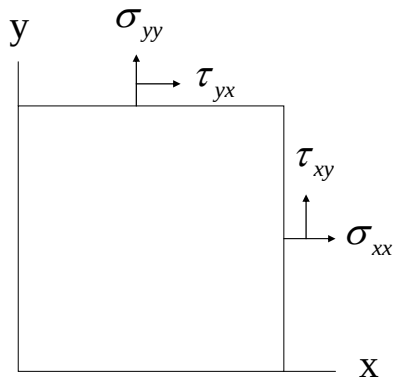

Figure 3. Stress Components in Two Dimensions

The stress is related to strain through the constitutive equation. The unit elongation or direct strain, ε_{ij}, is the deformation of a body as a result of the direct stress in the i direction. Likewise, the shearing strain, γ_{ij}, is the deformation as a result of shear stress. Shear strain can be thought of as the angle of deformation. The equations of motion are used to find displacements. Strain can be expressed in terms of derivatives of displacement. The following equations are the components of strain in a two-dimensional system (18:5-7):

$$\varepsilon_{xx} = \frac{\partial u}{\partial x} \; ; \; \varepsilon_{yy} = \frac{\partial v}{\partial y} \qquad 2.3.1$$

$$\gamma_{xy} = \frac{\partial u}{\partial y} + \frac{\partial v}{\partial x} \qquad 2.3.2$$

Given the components of strain, the components of stress can be derived using Hooke's Law and are expressed as

$$\sigma_{xx} = 2G\left(\frac{\upsilon}{1-2\upsilon}e + \varepsilon_{xx}\right) \qquad 2.3.3$$

$$\sigma_{yy} = 2G\left(\frac{\upsilon}{1-2\upsilon}e + \varepsilon_{yy}\right) \qquad 2.3.4$$

$$\sigma_{zz} = \upsilon\left(\sigma_{xx} + \sigma_{yy}\right)$$

$$\tau_{xy} = G\gamma_{xy} \qquad 2.3.5$$

with e defined in 2.2.5. Once functions for displacement are found, these equations are used to determine functions for stress and strain (18:5-7).

2.4 Stress Waves

When a load is applied to a medium, the material in the medium acts to relieve the pressure of the load. This action by the material to redistribute the pressure produces a wave called a stress wave. The speed of propagation for a stress wave is based on the material properties of the loaded region (18:485).

Unlike air, an elastic medium can be characterized by two types of waves, distortion and dilatation waves. Waves of distortion, or equivoluminal waves, produce deformation assuming the volume expansion is zero. Distortion waves consist of particle shearing and rotation only. Waves of dilatation, or irrotational waves, produce volume expansion. The speed of each wave type is characterized in terms of material properties without regard to the amount of force applied to the loaded region.

The stress wave speeds occur naturally in the equations of motion. For example, in 2.2.3 and 2.2.4, if the equations are divided through by G_2, the ratio $\frac{\rho_2}{G_2}$ appears, which is the inverse of the square distortion speed, $\frac{1}{c_2^2}$, which leads to the formula

$$c_2 = \sqrt{\frac{G_2}{\rho_2}} \qquad 2.4.1$$

Now, the dilatation wave speed, call it c_d, is directly related to the distortion speed for that material in the following manner:

$$c_d = \sqrt{\frac{\lambda + 2G}{\rho}}$$

where G is the shear modulus, λ is the Lamé's constant, and ρ is the density of the region of interest (18:487). The dilatation speed is not directly used in the formulation of the equations or the calculations of stress and strain in this document, since it can be shown to be proportional to the distortion speed (18:490). However, the distortion wave speed is inherent in the scaled equations of motion presented in a later section.

2.5 Continuity Conditions

At the interface between the rail (region II) and the coating (region I), several continuity conditions must be satisfied. First, the materials are considered to be perfectly bonded and maintain that bond through time. This implies we must have continuity of displacement for all x and time, t, or

$$u_1(x,0,t) = u_2(x,0,t) \qquad 2.5.1$$

$$v_1(x,0,t) = v_2(x,0,t) \qquad 2.5.2$$

The perfect bond assumed between the coating and the rail also leads to the continuity of shear and direct stress yielding

$$\tau_{xy_1}(x,0,t) = \tau_{xy_2}(x,0,t) \qquad 2.5.3$$

$$\sigma_{yy_1}(x,0,t) = \sigma_{yy_2}(x,0,t) \qquad 2.5.4$$

2.6 Initial and Boundary Conditions

The state of the system must be defined at $t = 0$. This study assumes quiescent initial conditions implying $u(x, y, 0) = v(x, y, 0) = 0$ and $u_t(x, y, 0) = v_t(x, y, 0) = 0$, where u_t is the first time derivative. As discussed in the previous chapter, the rail is considered infinite in length and is modeled as a half-space. This suggests a description of stress conditions as x and y approach infinity must be stated. This study assumes stress vanishes at infinity which leads to the conditions: $\sigma_{xx_1}, \sigma_{xx_2} \to 0$ as $|x| \to \infty$ and $\sigma_{yy_2} \to 0$ as $y \to -\infty$.

The impact load is introduced through boundary conditions applied at the top of the coating, $y = h$. The load is given in the form of stress as a function of position and time:

$$\tau_{xy_1}(x, h, t) = f(x - c_s t, t) H(l - |x - c_s t|) \qquad 2.6.1$$

$$\sigma_{yy_1}(x, h, t) = -k(x - c_s t, t) H(l - |x - c_s t|) \qquad 2.6.2$$

$$-\infty < x < \infty, \; t > 0$$

where $H(l - |x - c_s t|)$ is a Heaviside function piecewise defined as

$$H(l - |x - c_s t|) = \begin{cases} 0 & |x - c_s t| > l \\ 1 & |x - c_s t| \le l \end{cases}$$

This function represents the load moving at a velocity, c_s, in the direction of the positive x axis (see Figure 1). It acts as a switch to turn the loading off outside the region of the slipper of length $2l$.

2.7 Coordinate Transformation and Scaling

2.7.1 Moving Coordinate System

This study is primarily concerned with stress near or in the neighborhood of the moving load. For this reason, a moving coordinate system is introduced so the source is always centered about the origin. Verruijt and Cordova (16), Kennedy and Herrmann (11), and de Barros and Luco (10) use the same technique to ensure their moving loads stay near the origin. To ensure the proper frame of reference, the coordinate transformation $\xi = x - c_s t$ is introduced. Before the transformed equations are presented, the equations' dimensionless parameters are introduced and the equations are scaled.

2.7.2 Motivation for Scaling

Many mathematical problems inherently contain very large or small parameters. To take advantage of the size of parameters and to understand the contribution of each term relative to the size and strength of the parameters in the system of equations, it is necessary to introduce dimensionless parameters. In nondimensionalizing equations, reference values or "scales" are selected that are natural or "intrinsic" to the system (19:211). This system has three fundamental dimensions. They are mass (M), length (L), and time (T). All of the dimensioned quantities for the equations of motion can be written in terms of these fundamental dimensions. Table 1 shows the parameters and the values of interest for this problem along with their fundamental dimensions. It is necessary to know these values to understand why certain scales are chosen.

Parameter Name	Symbol	Range	Units	Fundamental Dimension
Density	ρ_1 ρ_2	1000-1500 7872	Kg/m^3	$M^1L^{-3}T^0$
Shear Modulus	G_1 G_2	$1.3x10^9$-$2.4x10^9$ $8x10^{10}$	Kg/ms^2	$M^1L^{-1}T^{-2}$
Shoe Speed	c_s	2000-3000	m/s	$M^0L^1T^{-1}$
Distortion Speed	c_1 c_2	1000-1300 3188	m/s	$M^0L^1T^{-1}$
Coating Thickness	h	$1.5x10^{-4}$-$1.8x10^{-3}$	m	$M^0L^1T^0$
Shoe Length	$2l$	0.2	m	$M^0L^1T^0$
Poisson's Ratio	υ_1 υ_2	0.3-0.45 0.29	dimensionless	$M^0L^0T^0$

Table 1. Dimensioned Parameter Values with Range, Units and Fundamental Dimension

2.7.3 Buckingham Pi/Dimension Analysis

In this section, theory is presented to show that finding the solutions to dimensionless equations of motion is equivalent to finding the solution to the original system. Then, using this theory, the dimensionless parameters are found that are natural to the system of differential equations, which leads to the scaled equations in the following section.

Let $f(q_1, q_2, ..., q_m) = 0$ be a *unit free* physical law, meaning that it is independent of the particular units, like British or metric, and $\{q_i\}_{i=1}^m$ be dimensioned quantities. Also, let $\{L_i\}_{j=1}^n$ be fundamental dimensions with $[q_i] = \prod_{j=1}^n L_j^{d_{ji}}$ for all $i = 1, 2, ..., m$, and D be an nxm dimension matrix with entries d_{ji}. If D has rank r then there are $k = m - r$

independent dimensionless quantities, $\pi_1, \pi_2, ..., \pi_k$, which are formed from $\{q_i\}_{i=1}^{m}$. The Buckingham Pi Theorem states that the law $f(q_1, q_2, ..., q_m) = 0$ is equivalent to $F(\pi_1, \pi_2, ..., \pi_k) = 0$ expressed in terms of the dimensionless quantities (19:195-221). Through dimension analysis the natural scales can be found by determining the dimensionless quantities for the system.

For this problem, the dimensioned quantities are $\{q_i\}_{i=1}^{7} = \{\rho_1, \rho_2, G_1, G_2, c_s, h, l\}$. Let $\pi = [\rho_1]^{\alpha_1}[\rho_2]^{\alpha_2}[G_1]^{\alpha_3}[G_2]^{\alpha_4}[c_s]^{\alpha_5}[h]^{\alpha_6}[l]^{\alpha_7} = M^{\beta_1}L^{\beta_2}T^{\beta_3}$, where π is any quantity made up of multiple powers of $\{q_i\}$ and [ ] mean the dimension of the listed quantity. Then define $\underline{\beta} = D\underline{\alpha}$, where $\underline{\alpha}$ and $\underline{\beta}$ are vectors of powers from the definition of π. With this definition, $\underline{\alpha}$ must be in the null space of D for π to be dimensionless. The dimension matrix for this problem is

$$D = \begin{matrix} \{\rho_1 & \rho_2 & G_1 & G_2 & c_s & h & l\} \end{matrix} \begin{bmatrix} 1 & 1 & 1 & 1 & 0 & 0 & 0 \\ -3 & -3 & -1 & -1 & 1 & 1 & 1 \\ 0 & 0 & -2 & -2 & -1 & 0 & 0 \end{bmatrix} \begin{Bmatrix} M \\ L \\ T \end{Bmatrix}$$

When the distortion speeds are removed, the columns of D correspond to the dimensioned quantities that occur in the differential equations and boundary conditions in the same order as Table 2.1. The rows of D correspond to the fundamental dimensions, mass, length, and time, respectively. The vectors in the braces are not part of the matrix D, but are references used to relate the entries in D to the actual parameters.

Now $rank(D) = 3$ which implies there are $k = 7 - 3 = 4$ independent dimensionless quantities, $\pi_1, \pi_2, \pi_3, \pi_4$.

Now to find the dimensionless quantities, four linearly independent vectors are chosen from the null space of D. Table 2 shows the vectors chosen with the dimensionless quantity produced.

	Null Space Vector	Dimensionless Quantity
π_1	$(0,0,0,0,0,1,-1)$	h/l
π_2	$\left(\frac{1}{2},0,-\frac{1}{2},0,1,0,0\right)$	$c_s\sqrt{\rho_1}/\sqrt{G_1}$
π_3	$(0,0,-1,1,0,0,0)$	G_2/G_1
π_4	$(-1,1,0,0,0,0,0)$	ρ_2/ρ_1

Table 2. Independent Dimensionless Quantities

Since $dim(\mathcal{N}(D)) = 4$, all other dimensionless quantities can be written as a product of powers of $\pi_1, \pi_2, \pi_3, \pi_4$.

2.7.4 Scaling

First an appropriate length scale is determined. With the presence of the thin coating, it is necessary to scale all parameters in the y direction by the thickness of the coating, h. However, the x direction is scaled by half the size of the slipper, l. The rail is modeled as a half-space and has no natural length scales. It will be scaled in the same manner as the coating region. Scaling the lengths in this manner leads to the small

dimensionless parameter, $\delta = \pi_1 = \frac{h}{l}$, which is on the order of 10^{-3} and can give insight into how terms are contributing to the equations of motion.

The fundamental dimension of mass occurs naturally in the density and shear modulus of the materials. However, from 2.4.1, it is seen that mass and density are related through the distortion speed. Further, by dividing the equations of motion, 2.2.1, 2.2.2, 2.2.3, and 2.2.4 through by their respective shear modulus, G_i, the inverse of the square distortion speed $\left(\frac{1}{c_i^2} = \frac{\rho_i}{G_i} \right)$ naturally appears. For these reasons, mass is scaled through the ratio of density to shear modulus introducing the speed scale, c_2, and given the material properties of both regions, a dimensionless speed is produced in the ratio of shoe speed to distortion speed, $c = \pi_2 \pi_3^{-1/2} \pi_4^{1/2} = \frac{c_s}{c_2}$.

There is another speed which occurs naturally and must be considered; the slipper speed or speed of the load, c_s. The slipper speed is more directly introduced into the equations of motion through the coordinate transformation, $\xi = x - c_s t$. With $\tilde{u}(\xi, y, t) = \tilde{u}(x - c_s t, y, t) = u(x, y, t)$, the acceleration term becomes

$$\frac{\partial^2 u}{\partial t^2} = c_s^2 \frac{\partial^2 \tilde{u}}{\partial \xi^2} - 2c_s \frac{\partial^2 \tilde{u}}{\partial \xi \partial t} + \frac{\partial^2 \tilde{u}}{\partial t^2}$$

Similarly with $\tilde{v}(\xi, y, t) = v(x, y, t)$

$$\frac{\partial^2 v}{\partial t^2} = c_s^2 \frac{\partial^2 \tilde{v}}{\partial \xi^2} - 2c_s \frac{\partial^2 \tilde{v}}{\partial \xi \partial t} + \frac{\partial^2 \tilde{v}}{\partial t^2}.$$

Thus a dimensionless slipper speed is necessary. To introduce this dimensionless speed, the slipper speed is scaled by the distortion speed in region I to define $\omega = \pi_2 = \frac{c_s}{c_1}$.

The last dimensioned quantity which is scaled is shear modulus because it naturally occurs in the interface conditions, 2.5.3 and 2.5.4. Both the shear modulus in region II and region I are scaled by the shear modulus in region I, which produces the dimensionless parameter $G = \pi_3 = \frac{G_2}{G_1}$. Now the parameters values from Table 2 are used to derive the acceptable ranges of the dimensionless parameters. These ranges are given in Table 3.

Symbol	Range
$\delta = h/l$	$1.5\text{x}10^{-3}$-$1.8\text{x}10^{-2}$
$c = c_s/c_2$	0.6-0.94
$G = G_2/G_1$	33-62
$\omega = c_s/c_1$	2-3
υ_1 υ_2	0.3-0.45 0.29

Table 3. Dimensionless Parameters and Ranges of Interest

The independent and dependent variables are also scaled. First the ξ and y coordinates are scaled by the lengths scales that correspond to their direction of motion. Additionally, time is scaled by $\frac{h}{c_1}$, the amount of time it takes the distortion wave in region I to travel through the thickness of the coating. This implies the dimensionless

independent variables are $\zeta = \frac{\xi}{l}$, $\eta = \frac{y}{h}$, and $\tau = \frac{c_1}{h}t$. With this transformation, $\eta = 0$ at the interface and $\eta = 1$ at the top of the coating.

Finally, the dependent variables, u and v, are scaled in the same way as ξ and y. That is, define

$$\frac{1}{l}u(x,y,t) = \hat{u}\left(\frac{x-c_s t}{l}, \frac{y}{h}, \frac{c_1 t}{h}\right) = \hat{u}(\zeta, \eta, \tau) \qquad 2.7.1$$

and

$$\frac{1}{h}v(x,y,t) = \hat{v}\left(\frac{x-c_s t}{l}, \frac{y}{h}, \frac{c_1 t}{h}\right) = \hat{v}(\zeta, \eta, \tau) \qquad 2.7.2$$

Now the moving coordinates and the set of dimensionless parameters are used to transform the equations of motion and the auxiliary conditions into an equivalent nondimensionalized system. By applying 2.7.1 and 2.7.2 to 2.2.1, 2.2.2, 2.2.3, and 2.2.4, the dimensionless equations of motion in the coating become

$$\delta^2\left(2\hat{g}(\eta)q_1 - \omega^2\right)\frac{\partial^2 \hat{u}_1}{\partial \zeta^2} + \hat{g}(\eta)\frac{\partial^2 \hat{u}_1}{\partial \eta^2} + \delta^2 \hat{g}(\eta)(r_1 + q_1)\frac{\partial^2 \hat{v}_1}{\partial \zeta \partial \eta} = -2\delta\omega\frac{\partial^2 \hat{u}_1}{\partial \zeta \partial \tau} + \frac{\partial^2 \hat{u}_1}{\partial \tau^2} \qquad 2.7.3$$

$$\delta^2\left(\hat{g}(\eta) - \omega^2\right)\frac{\partial^2 \hat{v}_1}{\partial \zeta^2} + 2\hat{g}(\eta)q_1\frac{\partial^2 \hat{v}_1}{\partial \eta^2} + \hat{g}(\eta)(r_1 + q_1)\frac{\partial^2 \hat{u}_1}{\partial \zeta \partial \eta} = -2\delta\omega\frac{\partial^2 \hat{v}_1}{\partial \zeta \partial \tau} + \frac{\partial^2 \hat{v}_1}{\partial \tau^2} \qquad 2.7.4$$

and in the rail become

$$\delta^2\left(2q_2 - c^2\right)\frac{\partial^2 \hat{u}_2}{\partial \zeta^2} + \frac{\partial^2 \hat{u}_2}{\partial \eta^2} + \delta^2(r_2 + q_2)\frac{\partial^2 \hat{v}_2}{\partial \zeta \partial \eta} = -2\frac{c^2}{\omega}\delta\frac{\partial^2 \hat{u}_2}{\partial \zeta \partial \tau} + \frac{c^2}{\omega^2}\frac{\partial^2 \hat{u}_2}{\partial \tau^2} \qquad 2.7.5$$

$$\delta^2\left(1 - c^2\right)\frac{\partial^2 \hat{v}_2}{\partial \zeta^2} + 2q_2\frac{\partial^2 \hat{v}_2}{\partial \eta^2} + (r_2 + q_2)\frac{\partial^2 \hat{u}_2}{\partial \zeta \partial \eta} = -2\frac{c^2}{\omega}\delta\frac{\partial^2 \hat{v}_2}{\partial \zeta \partial \tau} + \frac{c^2}{\omega^2}\frac{\partial^2 \hat{v}_2}{\partial \tau^2} \qquad 2.7.6$$

where

$$r_i = \frac{v_i}{1-2v_i};\ q_i = \frac{1-v_i}{1-2v_i} \quad i = 1,2 \tag{2.7.7}$$

Now the same transformations are applied to the continuity, boundary, and initial conditions. For continuity of displacement, these equations look exactly the same as the original functions:

$$\hat{u}_1(\zeta, 0, \tau) = \hat{u}_2(\zeta, 0, \tau) \tag{2.7.8}$$

$$\hat{v}_1(\zeta, 0, \tau) = \hat{v}_2(\zeta, 0, \tau) \tag{2.7.9}$$

It is now important to write stress in terms of 2.3.4 to include the scaled variables and parameters. Thus at $\eta = 0$, the continuity of shear stress becomes

$$\frac{\partial \hat{u}_1}{\partial \eta} + \delta^2 \frac{\partial \hat{v}_1}{\partial \zeta} = G\left(\frac{\partial \hat{u}_2}{\partial \eta} + \delta^2 \frac{\partial \hat{v}_2}{\partial \zeta} \right) \tag{2.7.10}$$

and the continuity of direct stress at $\eta = 0$ becomes

$$r_1 \frac{\partial \hat{u}_1}{\partial \zeta} + q_1 \frac{\partial \hat{v}_1}{\partial \eta} = G\left(r_2 \frac{\partial \hat{u}_2}{\partial \zeta} + q_2 \frac{\partial \hat{v}_2}{\partial \eta} \right) \tag{2.7.11}$$

At the upper boundary of the coating, $\eta = 1$, the loading conditions become

$$\frac{\partial \hat{u}_1}{\partial \eta} + \delta^2 \frac{\partial \hat{v}_1}{\partial \zeta} = \delta \hat{f}(\zeta, \tau) H(1 - |\zeta|) \tag{2.7.12}$$

and

$$r_1 \frac{\partial \hat{u}_1}{\partial \zeta} + q_1 \frac{\partial \hat{v}_1}{\partial \eta} = -\hat{k}(\zeta, \tau) H(1 - |\zeta|) \tag{2.7.13}$$

from (2.6.1) and (2.6.2) where $\hat{f}(\zeta,\tau)=\frac{1}{G_1}f\left(\frac{x-c_s t}{l},\frac{c_1 t}{h}\right)$ and

$\hat{k}(\zeta,\tau)=\frac{1}{2G_1}k\left(\frac{x-c_s t}{l},\frac{c_1 t}{h}\right)$. Notice that r_i and q_i are dimensionless and the functions f and k have the same dimensions as G_1, thus $\hat{f}$ and $\hat{k}$ are also dimensionless as their strength has been scaled by the shear modulus (G_1) in the coating. The vanishing stress conditions, $\hat{\sigma}_{\zeta_1},\hat{\sigma}_{\zeta_2}\to 0$ as $|\zeta|\to\infty$ and $\hat{\sigma}_{\eta_2}\to 0$ as $\eta\to-\infty$, are unchanged from the transform. Now at time $\tau=0$, the scaled quiescent initial conditions become $\hat{u}=\hat{v}=0$ and

$$\frac{\partial\hat{u}}{\partial\tau}-\delta\omega\frac{\partial\hat{u}}{\partial\zeta}=\frac{\partial\hat{v}}{\partial\tau}-\delta\omega\frac{\partial\hat{v}}{\partial\zeta}=0$$

2.8 Steady State System

The steady state solution comes from the system which is void of all time dependence. This implies as time progresses the system must see no change in the displacement with respect to time or position in the direction of motion. Mathematically, the right hand side of the equations of motion must be zero which implies

$$-2\omega\delta\frac{\partial\hat{u}_j}{\partial\zeta}+\frac{\partial\hat{u}_j}{\partial\tau}$$

and

$$-2\omega\delta\frac{\partial\hat{v}_j}{\partial\zeta}+\frac{\partial\hat{v}_j}{\partial\tau}$$

must both be constant. This thesis assumes the source of the impact load moves at a constant velocity. Physically this means the slipper has no acceleration because it is

traveling at its constant speed. Without acceleration, this research assumes the system has reached steady state and the equations of motion in the coating become

$$\delta^2\left(2\hat{g}(\eta)q_1-\omega^2\right)\frac{\partial^2\hat{u}_1}{\partial\zeta^2}+\hat{g}(\eta)\frac{\partial^2\hat{u}_1}{\partial\eta^2}+\delta^2\hat{g}(\eta)(r_1+q_1)\frac{\partial^2\hat{v}_1}{\partial\zeta\partial\eta}=0 \qquad 2.8.1$$

$$\delta^2\left(\hat{g}(\eta)-\omega^2\right)\frac{\partial^2\hat{v}_1}{\partial\zeta^2}+2\hat{g}(\eta)q_1\frac{\partial^2\hat{v}_1}{\partial\eta^2}+\hat{g}(\eta)(r_1+q_1)\frac{\partial^2\hat{u}_1}{\partial\zeta\partial\eta}=0 \qquad 2.8.2$$

and in the rail become

$$\delta^2\left(2q_2-c^2\right)\frac{\partial^2\hat{u}_2}{\partial\zeta^2}+\frac{\partial^2\hat{u}_2}{\partial\eta^2}+\delta^2(r_2+q_2)\frac{\partial^2\hat{v}_2}{\partial\zeta\partial\eta}=0 \qquad 2.8.3$$

$$\delta^2\left(1-c^2\right)\frac{\partial^2\hat{v}_2}{\partial\zeta^2}+2q_2\frac{\partial^2\hat{v}_2}{\partial\eta^2}+(r_2+q_2)\frac{\partial^2\hat{u}_2}{\partial\zeta\partial\eta}=0 \qquad 2.8.4$$

2.9 Summary

This chapter outlined the general theory governing the problem of interest. The theory led to a system of partial differential equations in terms of displacement to model the rail (region I) and the coating (region II) along with the load. Then the conditions necessary to solve the system 2.5.1-4 and 2.6.1,2 were presented. Next, the parameters of the system were used to find dimensionless quantities and the parameters were scaled to create dimensionless parameters (Table 3). Finally, the steady state equations were presented as the governing equations 2.8.1-4 to be solved in this study.

Chapter 3. Methodology and Solutions

3.1 Introduction

This chapter describes the methods used to solve the system of equations presented in Chapter 2. For comparison, the problem is first solved with the region II only, so that there is no coating and the force is applied directly to the rail. Since the system has an infinite domain in the direction of motion and vanishing stress applies, a Fourier transform is used to convert the equations to a system of ordinary differential equations. Since the loading is compactly supported, the system can be readily solved in the Fourier domain. Then the solution technique is described and the analytic solution is presented. Then an inverse Fourier transform is applied to obtain the solution in the spatial domain.

The transformed equations for the problem with coating are presented without detail since the method is identical to the no coating problem. A finite difference method is introduced to solve the equations numerically. This method produces solutions to the problem where the shear modulus varies through the thickness of the coating. The results for variable coating thickness and shear modulus are compared via their influence on the stress distribution at the interface.

3.2 Rail Only

In this section, the problem is solved with no coating applying the boundary conditions directly to the rail. The new boundary conditions are presented. A Fourier transform is introduced in the ζ direction and a homogenous linear system of first order

differential equations is set up and solved. Finally, the transform is inverted and the solutions for stress are presented rather than displacements.

3.2.1 New Boundary Condition

The equations of motion for the uncoated region II remain the same and are given by 2.8.3 and 2.8.4. However, with the coating removed, there is no longer a need for continuity conditions at the interface of the regions. Instead, the force is applied directly to the half-space. That is, the upper boundary is at $\eta = 0$, and the continuity of stress conditions at this boundary are

$$\delta \frac{\hat{\tau}_{\zeta\eta}(\zeta,\eta)}{G} = \frac{\partial \hat{u}_2}{\partial \eta} + \delta^2 \frac{\partial \hat{v}_2}{\partial \zeta} = \frac{\delta \hat{f}(\zeta)}{G} H\left(1-\left|\zeta\right|\right) \qquad 3.2.1$$

and

$$\frac{\hat{\sigma}_{\eta\eta}(\zeta,\eta)}{G} = r_2 \frac{\partial \hat{u}_2}{\partial \zeta} + q_2 \frac{\partial \hat{v}_2}{\partial \eta} = -\frac{\hat{k}(\zeta)}{G} H\left(1-\left|\zeta\right|\right) \qquad 3.2.2$$

3.2.2 Fourier Transform

To create a system of ordinary differential equations, first a spatial Fourier transform is introduced in the ζ direction. This transform is applied to the equations of motion as well as the boundary conditions. Since the rail is modeled as infinite in both directions, the Fourier transforms for the functions $\hat{u}$ and $\hat{v}$ are defined as

$$U(\alpha,\eta) = \int_{-\infty}^{\infty} e^{i\alpha\zeta} \hat{u}(\zeta,\eta) d\zeta \qquad 3.2.3$$

and

$$V(\alpha,\eta) = \int_{-\infty}^{\infty} e^{i\alpha\zeta} \hat{v}(\zeta,\eta) d\zeta \qquad 3.2.4$$

Notice, with this transform, all variables and parameters except for ζ are considered constant. Further, since the Fourier transform is a linear operator, each term in the equations can be transformed separately.

For demonstration purposes, the transform is performed on each term type in 2.8.3 and 2.8.4 with respect to the function $\hat{u}$:

$$\int_{-\infty}^{\infty} e^{i\alpha\zeta} \frac{\partial^2 \hat{u}(\zeta,\eta)}{\partial\zeta^2} d\zeta = -\alpha^2 U(\alpha,\eta)$$

$$\int_{-\infty}^{\infty} e^{i\alpha\zeta} \frac{\partial^2 \hat{u}(\zeta,\eta)}{\partial\eta^2} d\zeta = \frac{\partial^2 U(\alpha,\eta)}{\partial\eta^2}$$

$$\int_{-\infty}^{\infty} e^{i\alpha\zeta} \frac{\partial^2 \hat{u}(\zeta,\eta)}{\partial\zeta\partial\eta} d\zeta = i\alpha \frac{\partial U(\alpha,\eta)}{\partial\eta}$$

The boundary and continuity conditions are similarly transformed.

Thus, for every derivative of $\hat{u}$ and $\hat{v}$ with respect to two derivatives of ζ, the transformed function multiplies $-\alpha^2$ and its coefficient. And for every derivative of $\hat{u}$ and $\hat{v}$ with respect to one derivative of ζ, the transformed function multiplies $i\alpha$ and its coefficient. This produces the new system of ordinary differential equations in the Fourier domain:

$$-\alpha^2\delta^2\left(2q_2 - c^2\right)U_2 + \frac{d^2U_2}{d\eta^2} + i\alpha\delta^2(r_2 + q_2)\frac{dV_2}{d\eta} = 0 \qquad 3.2.5$$

$$-\alpha^2\delta^2\left(1 - c^2\right)V_2 + 2q_2\frac{d^2V_2}{d\eta^2} + i\alpha(r_2 + q_2)\frac{dU_2}{d\eta} = 0 \qquad 3.2.6$$

with the following conditions to satisfy:

$$i\alpha r_2 U_2 + q_2\frac{dV_2}{d\eta} \to 0, \text{ as } \eta \to -\infty \qquad 3.2.7$$

and at $\eta = 0$

$$\frac{dU_2}{d\eta} + i\alpha\delta^2 V_2 = \frac{\delta}{G} F(\alpha) \qquad 3.2.8$$

$$i\alpha r_2 U_2 + q_2 \frac{dV_2}{d\eta} = -\frac{1}{G} K(\alpha) \qquad 3.2.9$$

where

$$F(\alpha) = \int_{-1}^{1} e^{i\alpha\zeta} \hat{f}(\zeta) d\zeta \qquad 3.2.10$$

and

$$K(\alpha) = \int_{-1}^{1} e^{i\alpha\zeta} \hat{k}(\zeta) d\zeta \qquad 3.2.11$$

3.2.3 Eigenvalue-Eigenvector Approach

To find solutions for U and V, the equations of motion, 3.2.5 and 3.2.6, are converted to a homogeneous linear system of first order differential equations in the transform domain. First, let

$$\boldsymbol{W} = \begin{bmatrix} U \\ V \\ U_\eta \\ V_\eta \end{bmatrix} \qquad 3.2.12$$

Here the notation U_η indicates differentiation of U with respect to η. Then from 3.2.5 and 3.2.6,

$$\frac{d\boldsymbol{W}}{d\eta}=\begin{bmatrix}U_\eta\\V_\eta\\U_{\eta\eta}\\V_{\eta\eta}\end{bmatrix}=\begin{bmatrix}W_3\\W_4\\-\alpha^2\delta^2\left(2q_2-c^2\right)W_1-i\alpha\delta^2(r_2+q_2)W_4\\\frac{-\alpha^2\delta^2}{2q_2}\left(1-c^2\right)W_2-\frac{1}{2q_2}i\alpha(r_2+q_2)W_3\end{bmatrix}$$

where W_k is component k of the vector $\boldsymbol{W}$. Now let

$$Y=\begin{bmatrix}0&0&1&0\\0&0&0&1\\\alpha^2\delta^2\left(2q_2-c^2\right)&0&0&-i\alpha\delta^2(r_2+q_2)\\0&\frac{\alpha^2\delta^2}{2q_2}\left(1-c^2\right)&-\frac{1}{2q_2}i\alpha(r_2+q_2)&0\end{bmatrix} \qquad 3.2.13$$

then the equation becomes

$$\frac{d\boldsymbol{W}}{d\eta}=Y\boldsymbol{W} \qquad 3.2.14$$

This system has the solution

$$\boldsymbol{W}=\sum_{j=1}^{4}B_j\boldsymbol{x}_j e^{\lambda_j\eta}$$

where λ_j is the j^{th} eigenvalue of Y, $\boldsymbol{x}_j$ is an eigenvector associated with the j^{th} eigenvalue, and the B_j's are unknown coefficients. Further, the notation $x_j^{(k)}$ will mean the k^{th} component of the j^{th} eigenvector. Then, by the definition of $\boldsymbol{W}$,

$$U_2(\alpha,\eta)=\sum_{j=1}^{4}B_j x_j^{(1)}e^{\lambda_j\eta}$$

and

$$V_2(\alpha,\eta)=\sum_{j=1}^{4}B_j x_j^{(2)}e^{\lambda_j\eta}$$

Now, let $p_1 = \delta\sqrt{1-c^2}$ and $p_2 = \delta\sqrt{1-\frac{c^2}{2q_2}}$, then the eigenvalues of Y are $\lambda_{1,2} = \mp\alpha p_1$ and $\lambda_{3,4} = \mp\alpha p_2$ with corresponding eigenvectors

$$\boldsymbol{x}_{1,2} = \begin{bmatrix} 1 \\ \pm\frac{i}{p_1} \\ \lambda_{1,2} \\ -i\alpha \end{bmatrix} \text{ and } \boldsymbol{x}_{3,4} = \begin{bmatrix} 1 \\ \pm\frac{ip_2}{\delta^2} \\ \lambda_{3,4} \\ -\frac{ip_2^2}{\delta^2} \end{bmatrix}$$

Now the solutions are written as

$$U_2(\alpha,\eta) = B_1 e^{-\alpha p_1 \eta} + B_2 e^{\alpha p_1 \eta} + B_3 e^{-\alpha p_2 \eta} + B_4 e^{\alpha p_2 \eta} \qquad 3.2.15$$

and

$$V_2(\alpha,\eta) = B_1 \frac{i}{p_1} e^{-\alpha p_1 \eta} - B_2 \frac{i}{p_1} e^{\alpha p_1 \eta} + B_3 \frac{ip_2}{\delta^2} e^{-\alpha p_2 \eta} - B_4 \frac{ip_2}{\delta^2} e^{\alpha p_2 \eta} \qquad 3.2.16$$

With the form of the solution known, it is necessary to apply the boundary conditions to find the unknown coefficients. First, consider the vanishing stress condition as $\eta \to -\infty$. Applying 3.2.15 and 3.2.16 to 3.2.7 implies

$$i\alpha r_2 U_2 + q_2 \frac{dV_2}{d\eta} = -i\alpha\left[B_1 e^{-\alpha p_1 \eta} + B_2 e^{\alpha p_1 \eta}\right] + i\alpha\left(r_2 - \frac{p_2^2 q_2}{\delta^2}\right)\left[B_3 e^{-\alpha p_2 \eta} + B_4 e^{\alpha p_2 \eta}\right]$$

which must vanish as $\eta \to -\infty$. This gives rise to two cases to consider, $\alpha > 0$ and $\alpha < 0$. First observe, p_1 and p_2 are always positive for the values of the parameters this study discusses and η is always negative. Thus, for $\alpha > 0$, require $B_1 = B_3 = 0$ or the stress would grow exponentially as $\eta \to -\infty$. Likewise, for $\alpha < 0$, require $B_2 = B_4 = 0$. This reduces the solutions for displacement to

$$U_2(\alpha,\eta) = \beta_1 e^{|\alpha| p_1 \eta} + \beta_2 e^{|\alpha| p_2 \eta} \qquad 3.2.17$$

and

$$V_2(\alpha,\eta) = \left[\frac{i}{p_1} \beta_1 e^{|\alpha| p_1 \eta} + \frac{i p_2}{\delta^2} \beta_2 e^{|\alpha| p_2 \eta} \right] \mathrm{sgn}(-\alpha) \qquad 3.2.18$$

where $\mathrm{sgn}(-\alpha)$ is the sign of $-\alpha$, and β_1 and β_2 are unknown coefficients.

3.2.4 Determining the Coefficients

To find β_1 and β_2, 3.2.8 and 3.2.9 are applied to the general solution, 3.2.17 and 3.2.18. Let $\boldsymbol{U}_k = \begin{bmatrix} U \\ V \end{bmatrix}$ in region k. Then for convenience the boundary conditions are written in matrix form:

$$\begin{bmatrix} 1 & 0 \\ 0 & q_2 \end{bmatrix} \frac{d\boldsymbol{U}_2}{d\eta} + \begin{bmatrix} 0 & i\alpha\delta^2 \\ i\alpha r_2 & 0 \end{bmatrix} \boldsymbol{U}_2 = \begin{bmatrix} \dfrac{\delta F}{G} \\ \dfrac{-K}{G} \end{bmatrix} \qquad 3.2.19$$

From 3.2.17 and 3.2.18,

$$\boldsymbol{U}_2 = \chi \begin{bmatrix} e^{|\alpha| p_1 \eta} & 0 \\ 0 & e^{|\alpha| p_2 \eta} \end{bmatrix} \boldsymbol{\beta} \qquad 3.2.20$$

where $\boldsymbol{\beta} = \begin{bmatrix} \beta_1 \\ \beta_2 \end{bmatrix}$ and

$$\chi = \begin{bmatrix} 1 & 1 \\ \dfrac{i}{p_1}\mathrm{sgn}(-\alpha) & \dfrac{i p_2}{\delta^2}\mathrm{sgn}(-\alpha) \end{bmatrix} \qquad 3.2.21$$

Thus $\boldsymbol{U}_2(\alpha,0) = \chi\boldsymbol{\beta}$ and

$$\frac{d\boldsymbol{U}_2}{d\eta}(\alpha,0)=\chi\begin{bmatrix}|\alpha|\,p_1 & 0\\ 0 & |\alpha|\,p_2\end{bmatrix}\boldsymbol{\beta}$$

Substituting this into 3.2.19 results in the equation

$$G\left\{\begin{bmatrix}1 & 0\\ 0 & q_2\end{bmatrix}\chi\begin{bmatrix}|\alpha|\,p_1 & 0\\ 0 & |\alpha|\,p_2\end{bmatrix}+\begin{bmatrix}0 & i\alpha\delta^2\\ i\alpha r_2 & 0\end{bmatrix}\chi\right\}\boldsymbol{\beta}=\begin{bmatrix}\delta F\\ -K\end{bmatrix} \qquad 3.2.22$$

which can be reduced to

$$Q\boldsymbol{\beta}=\begin{bmatrix}\dfrac{\delta F}{|\alpha|G}\\ \dfrac{-iK}{\alpha G}\end{bmatrix}$$

with Q defined in Appendix A. Solving for $\boldsymbol{\beta}$ and substituting into 3.2.20 produces

$$\boldsymbol{U}_2(\alpha,\eta)=\frac{1}{G}\chi\begin{bmatrix}e^{|\alpha|p_1\eta} & 0\\ 0 & e^{|\alpha|p_2\eta}\end{bmatrix}Q^{-1}\begin{bmatrix}\dfrac{\delta}{|\alpha|} & 0\\ 0 & -\dfrac{i}{\alpha}\end{bmatrix}\begin{bmatrix}F\\ K\end{bmatrix} \qquad 3.2.23$$

which implies

$$\boldsymbol{U}_2(\alpha,\eta)=\frac{1}{G\det(Q)}\begin{bmatrix}\dfrac{\delta}{|\alpha|}\left(Q_2e^{|\alpha|p_1\eta}+e^{|\alpha|p_2\eta}\right) & \dfrac{i}{\alpha}\left(p_2e^{|\alpha|p_1\eta}-Q_1e^{|\alpha|p_2\eta}\right)\\ \dfrac{-i}{\alpha}\left(\dfrac{\delta Q_2}{p_1}e^{|\alpha|p_1\eta}+\dfrac{p_2}{\delta}e^{|\alpha|p_2\eta}\right) & \dfrac{1}{|\alpha|}\left(\dfrac{p_2}{p_1}e^{|\alpha|p_1\eta}-\dfrac{p_2Q_1}{\delta^2}e^{|\alpha|p_2\eta}\right)\end{bmatrix}\begin{bmatrix}F\\ K\end{bmatrix} \qquad 3.2.24$$

where $Q_1=\dfrac{p_1^2+\delta^2}{p_1}$ and $Q_2=r_2-\dfrac{p_2^2}{\delta^2}$. Writing the solution in this form breaks $\boldsymbol{U}_2$ into the coefficients of F and K. Now the influence of direct and shear stress on displacement can be seen immediately.

3.2.5 Inverting the Transform

The inverse Fourier transform of 3.2.24 is applied only to the coefficients of F and K, since the Fourier inverted coefficients can be convolved with the functions $\hat{f}$ and $\hat{k}$ outside the transform domain to obtain the solution. Further, this research is interested in stress. Consequently, the equations for stress in the transform domain are written using the displacement solutions and the inverse transform is applied to the stress. Similar to the left hand sides of 3.2.8 and 3.2.9, the Fourier transformed equations for stress are

$$\ddot{\sigma}_{\zeta\zeta} = 2G\left(i\alpha q_2 U_2 + r_2 \frac{dV_2}{d\eta} \right)$$

$$\ddot{\sigma}_{\eta\eta} = 2G\left(i\alpha r_2 U_2 + q_2 \frac{dV_2}{d\eta} \right)$$

$$\ddot{\tau}_{\zeta\eta} = G\left(\frac{dU_2}{d\eta} + i\alpha\delta^2 V_2 \right)$$

Now substituting the solution 3.2.24 into these equations gives

$$\ddot{\sigma}_{\zeta\zeta} = \frac{2}{det(Q)} \begin{bmatrix} Q_2 e^{|\alpha| p_1 \eta} + \left(q_2 - \frac{p_2^2}{\delta^2} r_2 \right) e^{|\alpha| p_2 \eta} \\ -p_2 e^{|\alpha| p_1 \eta} + Q_1 \left(q_2 - \frac{p_2^2}{\delta^2} r_2 \right) e^{|\alpha| p_2 \eta} \end{bmatrix}^T \begin{bmatrix} i\delta \,\mathrm{sgn}(\alpha) & 0 \\ 0 & 1 \end{bmatrix} \begin{bmatrix} F \\ K \end{bmatrix} \qquad 3.2.25$$

$$\ddot{\sigma}_{\eta\eta} = \frac{2}{det(Q)} \begin{bmatrix} -Q_2 e^{|\alpha| p_1 \eta} + \left(r_2 - \frac{p_2^2}{\delta^2} q_2 \right) e^{|\alpha| p_2 \eta} \\ p_2 e^{|\alpha| p_1 \eta} + Q_1 \left(r_2 - \frac{p_2^2}{\delta^2} q_2 \right) e^{|\alpha| p_2 \eta} \end{bmatrix}^T \begin{bmatrix} i\delta \,\mathrm{sgn}(\alpha) & 0 \\ 0 & 1 \end{bmatrix} \begin{bmatrix} F \\ K \end{bmatrix} \qquad 3.2.26$$

$$\ddot{\tau}_{\zeta\eta} = \frac{1}{det(Q)} \begin{bmatrix} Q_2 \dfrac{p_1^2 + \delta^2}{p_1} e^{|\alpha| p_1 \eta} + 2 p_2 e^{|\alpha| p_2 \eta} \\ \dfrac{p_1^2 + \delta^2}{p_1} e^{|\alpha| p_1 \eta} - 2 Q_1 e^{|\alpha| p_2 \eta} \end{bmatrix}^T \begin{bmatrix} \delta & 0 \\ 0 & i p_2 \operatorname{sgn}(\alpha) \end{bmatrix} \begin{bmatrix} F \\ K \end{bmatrix} \qquad 3.2.27$$

Notice, other than constants, there are two term types that occur in the stresses; $ik_1 \operatorname{sgn}(\alpha) e^{|\alpha| k_2 \eta}$ and $k_1 e^{|\alpha| k_2 \eta}$. Therefore, the inverse Fourier transform is performed on each term type and the results are applied to 3.2.25, 3.2.26, 3.2.27.

Define the inverse Fourier transform as

$$\mathcal{F}^{-1}(f(\alpha)) = \frac{1}{2\pi} \int_{-\infty}^{\infty} f(\alpha) e^{-i\alpha\zeta} d\alpha$$

Then

$$\mathcal{F}^{-1}(ik_1 \operatorname{sgn}(\alpha) e^{|\alpha| k_2 \eta}) =$$

$$\frac{1}{2\pi} \int_{-\infty}^{\infty} ik_1 \operatorname{sgn}(\alpha) e^{|\alpha| k_2 \eta} e^{-i\alpha\zeta} d\alpha =$$

$$\frac{ik_1}{2\pi} \int_0^{\infty} e^{\alpha(k_2\eta - i\zeta)} + e^{\alpha(-k_2\eta - i\zeta)} d\alpha = \frac{k_1}{\pi} \frac{\zeta}{k_2^2 \eta^2 + \zeta^2}$$

and

$$\mathcal{F}^{-1}(k_1 e^{|\alpha| k_2 \eta}) =$$

$$\frac{1}{2\pi} \int_{-\infty}^{\infty} k_1 e^{|\alpha| k_2 \eta} e^{-i\alpha\zeta} d\alpha =$$

$$\frac{k_1}{2\pi} \int_0^{\infty} e^{\alpha(k_2\eta - i\zeta)} + e^{\alpha(-k_2\eta - i\zeta)} d\alpha = \frac{k_1 k_2}{\pi} \frac{\eta}{k_2^2 \eta^2 + \zeta^2}$$

Let $Z_i(\zeta,\eta)=\dfrac{\zeta}{p_i^2\eta^2+\zeta^2}$ and $N_i(\zeta,\eta)=\dfrac{\eta}{p_i^2\eta^2+\zeta^2}$ for $i=1,2$, then inverse Fourier transforms for the stresses are

$$\hat{\sigma}_{\zeta\zeta}=\frac{2}{\pi det(Q)}\Bigg[\delta\left(Q_2Z_1(\zeta,\eta)+\left(q_2-\frac{p_2^2}{\delta^2}r_2\right)Z_2(\zeta,\eta)\right)*\hat{f}+ p_2\left(p_1N_1(\zeta,\eta)-Q_1\left(q_2-\frac{p_2^2}{\delta^2}r_2\right)N_2(\zeta,\eta)\right)*\hat{k}\Bigg] \tag{3.2.28}$$

$$\hat{\sigma}_{\eta\eta}=\frac{2}{\pi det(Q)}\Bigg[\delta\left(-Q_2Z_1(\zeta,\eta)+\left(r_2-\frac{p_2^2}{\delta^2}q_2\right)Z_2(\zeta,\eta)\right)*\hat{f}+ p_2\left(-p_1N_1(\zeta,\eta)-Q_1\left(r_2-\frac{p_2^2}{\delta^2}q_2\right)N_2(\zeta,\eta)\right)*\hat{k}\Bigg] \tag{3.2.29}$$

$$\hat{\tau}_{\zeta\eta}=\frac{2}{\pi det(Q)}\Big[-\delta\left(Q_2\left(p_1^2+\delta^2\right)N_1(\zeta,\eta)+2p_2^2N_2(\zeta,\eta)\right)*\hat{f}+ p_2Q_1\left(Z_1(\zeta,\eta)-2Z_2(\zeta,\eta)\right)*\hat{k}\Big] \tag{3.2.30}$$

where $(*)$ is the convolution operator defined as

$$f*g=\int_{-\infty}^{\infty}f(\zeta)g(\zeta-x)d\zeta$$

Recall that the functions $\hat{f}$ and $\hat{k}$ are the loading functions at the surface. In this study, three loading functions are used to describe the stress distribution in the rail in Chapter 4. The convolutions of the solution in the rail with the loading functions are given in Appendix B.

3.3 Coated Rail Analytic Solution

In this section, the problem is solved with the coating on the half-space. The solution procedure follows that of section 3.2. The solution in the spatial Fourier domain is introduced and a homogenous linear system of first order differential equations is set up and solved for the rail and coating. Unknown coefficients are found by applying the boundary and interface conditions.

3.3.1 Solution in the Fourier Domain

To write the equations of motion in region I in matrix form, first divide 2.8.1 and 2.8.2 through by $\hat{g}(\eta)$ and make some convenient substitutions. Let

$$a = a(\eta) = \alpha^2\delta^2\left(2q - \frac{\omega^2}{\hat{g}(\eta)}\right)$$

$$b_1 = i\alpha\delta^2(r+q)$$

$$b_2 = i\alpha(r+q)$$

$$c = c(\eta) = \alpha^2\delta^2\left(1 - \frac{\omega^2}{\hat{g}(\eta)}\right)$$

where ω and δ are defined in Table 3 and r and q are define in 2.7.7. As with the uncoated problem equations, 2.8.1 and 2.8.2, are spatially Fourier transformed to produce

$$\begin{bmatrix} 1 & 0 \\ 0 & 2q \end{bmatrix}\frac{d^2\boldsymbol{U}_1}{d\eta^2} + \begin{bmatrix} 0 & b_1 \\ b_2 & 0 \end{bmatrix}\frac{d\boldsymbol{U}_1}{d\eta} - \begin{bmatrix} a & 0 \\ 0 & c \end{bmatrix}\boldsymbol{U}_1 = 0 \qquad 3.3.1$$

for $0 < \eta < 1$. The boundary conditions at the top of the coating, $\eta = 1$, is similar to 3.2.19 and becomes

$$\begin{bmatrix} 1 & 0 \\ 0 & q \end{bmatrix}\frac{d\boldsymbol{U}_1}{d\eta}(\alpha,1) + \begin{bmatrix} 0 & i\alpha\delta^2 \\ i\alpha r & 0 \end{bmatrix}\boldsymbol{U}_1(\alpha,1) = \begin{bmatrix} \delta F \\ -K \end{bmatrix} \qquad 3.3.2$$

where F and K are defined in 3.2.10 and 3.2.11. At $\eta = 0$, the continuity of displacement becomes

$$\boldsymbol{U}_1(\alpha,0) = \boldsymbol{U}_2(\alpha,0) \tag{3.3.3}$$

and the continuity of stress becomes

$$\begin{bmatrix} 1 & 0 \\ 0 & q_1 \end{bmatrix} \frac{d\boldsymbol{U}_1}{d\eta}(\alpha,0) + \begin{bmatrix} 0 & i\alpha\delta^2 \\ i\alpha r_1 & 0 \end{bmatrix} \boldsymbol{U}_1(\alpha,0) = G\left(\begin{bmatrix} 1 & 0 \\ 0 & q_2 \end{bmatrix} \frac{d\boldsymbol{U}_2}{d\eta}(\alpha,0) + \begin{bmatrix} 0 & i\alpha\delta^2 \\ i\alpha r_2 & 0 \end{bmatrix} \boldsymbol{U}_2(\alpha,0) \right) \tag{3.3.4}$$

This system of equations is converted to a linear system of differential equations using 3.2.12 to produce 3.2.14 with Y now defined as

$$Y = \begin{bmatrix} 0 & 0 & 1 & 0 \\ 0 & 0 & 0 & 1 \\ \alpha^2\delta^2\left(2q_1 - \dfrac{\omega^2}{\hat{g}(\eta)}\right) & 0 & 0 & i\alpha\delta^2(r_1+q_1) \\ 0 & \dfrac{\alpha^2\delta^2}{2q_1}\left(1 - \dfrac{\omega^2}{\hat{g}(\eta)}\right) & \dfrac{i\alpha}{2q_1}(r_1+q_1) & 0 \end{bmatrix} \tag{3.3.5}$$

If there is a variation in the shear modulus ($\hat{g}(\eta)$ is non constant), then the system must be solved numerically. However, if the coating is uniform then $\hat{g}(\eta) \equiv 1$, and the system has a general solution similar to the no coating problem. Thus the general solutions for displacements in the coating are

$$U_1(\alpha,\eta) = \sum_{j=1}^{4} A_j x_j^{(1)} e^{\lambda_j \eta} \tag{3.3.6}$$

and

$$V_1(\alpha,\eta) = \sum_{j=1}^{4} A_j x_j^{(2)} e^{\lambda_j \eta} \tag{3.3.7}$$

Let $m_1 = i\delta\sqrt{\omega^2 - 1}$ and $m_2 = \delta\sqrt{1 - \frac{\omega^2}{2q_1}}$, then the eigenvalues are $\lambda_{1,2} = \mp\alpha m_1$ and $\lambda_{3,4} = \mp\alpha m_2$ with associated eigenvectors

$$\boldsymbol{x}_{1,2} = \begin{bmatrix} 1 \\ \pm\frac{1}{m_1} \\ \lambda_{1,2} \\ -i\alpha \end{bmatrix} \text{ and } \boldsymbol{x}_{3,4} = \begin{bmatrix} 1 \\ \pm\frac{im_2}{\delta^2} \\ \lambda_{3,4} \\ -\frac{im_2^2}{\delta^2} \end{bmatrix} \qquad 3.3.8$$

The general solution for the rail is given by equations 3.2.17 and 3.2.18. All that remains is to find $A_1, A_2, A_3, A_4, \beta_1$, and β_2.

3.3.2 Determining the Coefficients

The coefficients $A_1, A_2, A_3, A_4, \beta_1$, and β_2 are determined by satisfying the load conditions at the top of the coating, 3.3.2, and the interface conditions, 3.3.3 and 3.3.4. After these equations are transformed and the general solutions, given by 3.2.17, 3.2.18, 3.3.6, and 3.3.7, are introduced, a linear system for the coefficients emerge. This equation has the form

$$\begin{bmatrix} R_1 & R_2 \\ L & 0_{2x2} \end{bmatrix} \begin{bmatrix} \boldsymbol{A} \\ \boldsymbol{\beta} \end{bmatrix} = \begin{bmatrix} \boldsymbol{0} \\ \boldsymbol{F} \end{bmatrix} \qquad 3.3.9$$

Here $\boldsymbol{A}$ is a vector of the four unknown coefficients associated with the coated region solution and $\boldsymbol{\beta}$ the coefficients associated with the rail region solution. The first four elements of the forcing vector are all zero while the last are comprised in $\mathbf{F} = \begin{bmatrix} \delta F \\ -K \end{bmatrix}$, where F and K are defined in 3.2.10 and 3.2.11. The matrix is comprised of sub

blocks, R_1, R_2, L given in Appendix C. R_1 and R_2 together form a 4x6 block derived from the interface conditions at $\eta = 0$. The L block is derived from the loading stress conditions at $\eta = 1$.

With the aid of Mathematica™, the solutions to 3.3.9 can be determined. However, the results are cumbersome and not suitable for transform inversion. Instead the solution to 3.3.9 is found for selected parameters. The resulting coefficients can be used in 3.2.17, 3.2.18, 3.3.6, and 3.3.7 to determine the displacements (in the transform domain) through the thickness of the coating and in the rail. These results are used to validate a numerical approach.

3.4 Finite Difference Method/Coated System

To handle coatings which may vary through the thickness, it is necessary to use a numerical method to investigate displacements in the coating and their influence on the stress distribution in the half-space.

3.4.1Method Derivation

The differential equations in the coating are written in terms of central differences to obtain $O\left(h^2\right)$ approximations, where the interval $\eta = [0,1]$ is partitioned into n subintervals of size $h = 1/n$. For the rest of this section, subscripts are no longer used to identify region. Unless otherwise noted, all constants and functions are for the coating (region I). First, let $\boldsymbol{U}_i = \boldsymbol{U}\left(\eta_i\right)$ be the displacement vector at the i^{th} partition starting at $\eta = 0$ and $\eta_i = kh$, $k = 0,1,...,n$, be the size of each partition. Then central differences for each derivative term are

$$\left.\frac{d^2\boldsymbol{U}}{d\eta^2}\right|_{\eta=\eta_i} \approx \frac{1}{h^2}\left\{\boldsymbol{U}_{k+1} - 2\boldsymbol{U}_k + \boldsymbol{U}_{k\text{-}1}\right\}$$

and

$$\left.\frac{d\boldsymbol{U}}{d\eta}\right|_{\eta=\eta_i} \approx \frac{1}{2h}\left\{\boldsymbol{U}_{k+1} - \boldsymbol{U}_{k\text{-}1}\right\}$$

Then from 3.3.1, the central difference formula for the equations of motion become

$$\begin{bmatrix} 1 & \frac{b_1 h}{2} \\ \frac{b_2 h}{2} & 2q \end{bmatrix}\boldsymbol{U}_{k+1} - \begin{bmatrix} a_k h^2 + 2 & 0 \\ 0 & c_k h^2 + 4q \end{bmatrix}\boldsymbol{U}_k + \begin{bmatrix} 1 & -\frac{b_1 h}{2} \\ -\frac{b_2 h}{2} & 2q \end{bmatrix}\boldsymbol{U}_{k-1} = 0 \qquad 3.4.1$$

for $k = 0,1,2,...,n$ where $k = 0$ corresponds to the interface between the coating and the rail, $\eta = 0$, and $k = n$ corresponds to the top of the coating, $\eta = 1$.

When $i = 0$, equation 3.4.1 requires knowledge of $\boldsymbol{U}_{-1}$ (i.e. $\boldsymbol{U}(-h)$). Also at $k = n$, 3.4.1 requires $\boldsymbol{U}_{n+1}$ $\left(\boldsymbol{U}(1+h)\right)$. These values are from *ghost* points used in the calculations and are determined from the boundary and interface conditions.

Now the boundary conditions are converted to central differences as well. First, at $\eta = 1$, the condition becomes

$$\begin{bmatrix} 1 & 0 \\ 0 & q \end{bmatrix}\frac{1}{2h}\left[\boldsymbol{U}_{n+1} - \boldsymbol{U}_{n\text{-}1}\right] + \begin{bmatrix} 0 & i\alpha\delta^2 \\ i\alpha r & 0 \end{bmatrix}\boldsymbol{U}_n = \begin{bmatrix} \delta F \\ -K \end{bmatrix}$$

which implies

$$\boldsymbol{U}_{n+1} = \boldsymbol{U}_{n-1} - 2i\alpha h\begin{bmatrix} 0 & \delta^2 \\ \frac{r}{q} & 0 \end{bmatrix}\boldsymbol{U}_n + 2h\begin{bmatrix} \delta F \\ \frac{-K}{q} \end{bmatrix} \qquad 3.4.2$$

Substituting into 3.4.1 for to $k = n$ produces

$$2\begin{bmatrix}1 & 0\\ 0 & 2q\end{bmatrix}\boldsymbol{U}_{n-1}-\begin{bmatrix}ah^2+2+\dfrac{ib_1\alpha rh^2}{q} & 2i\alpha\delta^2 h\\ 4i\alpha rh & ch^2+4q+i\alpha\delta^2 b_2h^2\end{bmatrix}\boldsymbol{U}_n=$$
$$-2h\begin{bmatrix}1 & \dfrac{b_1h}{2}\\ \dfrac{b_2h}{2} & 2q\end{bmatrix}\begin{bmatrix}\delta F\\ \dfrac{-K}{q}\end{bmatrix} \qquad 3.4.3$$

At $\eta=0$, the boundary condition is more complex to derive since the solution in the rail for the coupled system is not known. However, the form of the solution is the general form of the solution in the rail is given by 3.2.20. To evaluate the solution numerically in the coating, it is necessary to eliminate dependencies on $\boldsymbol{U}_2(\alpha,0)$ in the rail using the known form of the rail solution. First, applying the boundary condition 3.3.3 and the known solution 3.2.20 produces

$$\boldsymbol{U}_1(\alpha,0)=\chi\boldsymbol{\beta}=\boldsymbol{U}_2(\alpha,0)$$

with χ given by 3.2.21. For the parameter ranges of interest, χ is always invertible, which implies

$$\boldsymbol{\beta}=\chi^{-1}\boldsymbol{U}_1(\alpha,0) \qquad 3.4.4$$

Next, apply the continuity of stress condition in 3.3.4. First observe that the right hand side of 3.3.4 is simply the left hand side of 3.2.22. Using 3.4.4 for $\boldsymbol{\beta}$ in the left hand side of 3.2.22 and substituting into 3.3.4 produces the new form of the boundary condition:

$$\begin{bmatrix}1 & 0\\ 0 & q_1\end{bmatrix}\frac{d\boldsymbol{U}_2}{d\eta}(\alpha,0)+\boldsymbol{H}\boldsymbol{U}_2(\alpha,0)=\begin{bmatrix}0\\ 0\end{bmatrix} \qquad 3.4.5$$

where $\boldsymbol{H}$ captures the influence of the rail on the coating. $\boldsymbol{H}$ is given in Appendix D. Now, introduce the finite differences at $\eta = 0$ to produce

$$\frac{1}{2h}\begin{bmatrix} 1 & 0 \\ 0 & q_1 \end{bmatrix}(\boldsymbol{U}_1 - \boldsymbol{U}_{-1}) + \boldsymbol{H}\boldsymbol{U}_0 = \begin{bmatrix} 0 \\ 0 \end{bmatrix}$$

or

$$\boldsymbol{U}_{-1} = \boldsymbol{U}_1 + 2h\begin{bmatrix} 1 & 0 \\ 0 & \dfrac{1}{q_1} \end{bmatrix}\boldsymbol{H}\boldsymbol{U}_0$$

Substituting this into 3.4.1, with $i = 0$ produces the effective boundary condition

$$2\begin{bmatrix} 1 & 0 \\ 0 & 2q \end{bmatrix}\boldsymbol{U}_1 - \hat{G}\boldsymbol{U}_0 = \begin{bmatrix} 0 \\ 0 \end{bmatrix} \qquad 3.4.6$$

with $\hat{G}$ given in Appendix D.

3.4.1, 3.4.3, and 3.4.6 are the equations necessary for the finite difference code.

3.4.1 Code Validation

When $\hat{g}(\eta) \equiv 1$, the finite difference code solves the same system of equations as the analytic solution described in section 3.3, the coated rail problem. Thus, the finite difference code can be compared to the analytic solution for selected values of parameters. The solutions are compared over the entire range of parameter values of interest to this study. Figure 4 illustrates the convergence of the finite difference algorithm as the number of partitions in the coating increase, with parameters δ, υ_1, υ_2, c, ω, G, F, and K set to 10^{-3}, 0.4, 0.29, 0.9, 3, 60, 1, and 1, respectively. At $n = 100$, the curve associated with the exact solution and that of the finite difference

solution agree almost exactly over the range of $-10 \le \alpha \le 10$. These curves are a plot of the transformed U displacement in the complex U plane. Curves corresponding to $n = 5, 10, \text{and } 100$ are shown for comparison.

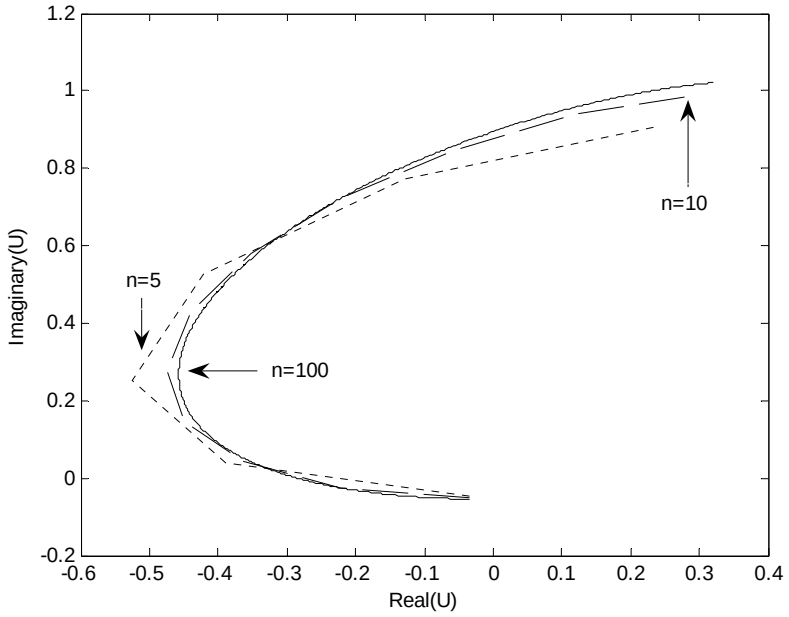

Figure 4. Demonstration of Finite Difference Code Convergence for Select Parameter Values

During the test for convergence, it was discovered that a certain parameter combination, the product $\alpha\delta$, had the greatest affect on error. As the product $\alpha\delta$ grows in magnitude, the number of partitions of the interval $0 < \eta < 1$ needed to maintain a specified accuracy must grow as well. This study seeks to have the relative error less than 10^{-4}. Figure 5 shows the number of partitions needed for convergence to the true solution within a specified level of accuracy versus the product $\alpha\delta$. The level of accuracy, given by relative error, is labeled on each curve. For example, with $\alpha\delta = 0.7$,

follow the dashed line from the $\alpha\delta$ axis up to the curve corresponding to a relative error of 10^{-5}. Then follow the dashed line to the axis corresponding to the number of partitions to get $n = 26$, partitions needed for $\alpha\delta = 0.7$ with a relative error of 10^{-5}.

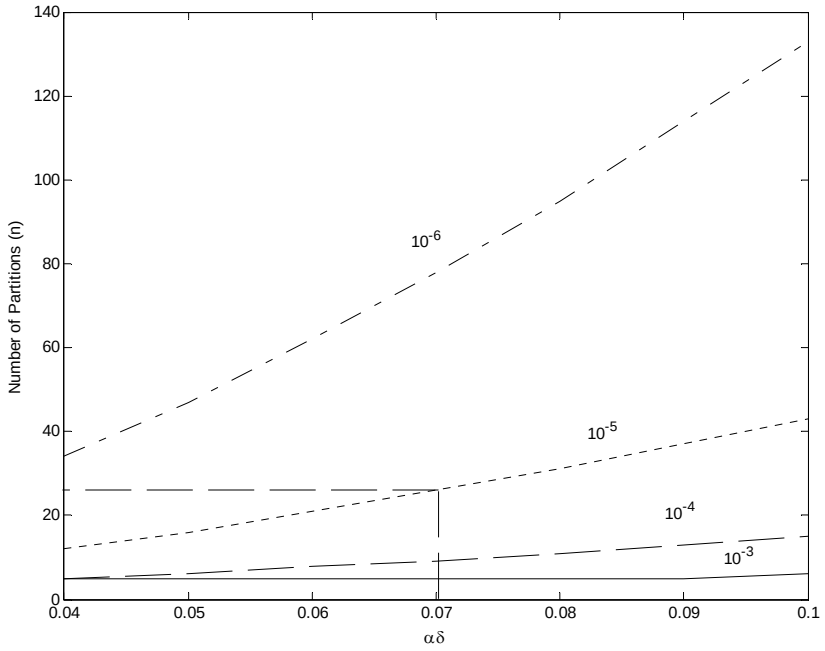

Figure 5. Number of Partitions Needed for Code Convergence
With Respect to Relative Error

For this study, $n = 15$ is an acceptable number of partitions to obtain relative error less than 10^{-4}.

3.5 Summary

This chapter began with a discussion of the rail only problem. A spatial Fourier transform was introduced in the ζ direction which led to a homogeneous linear system of ordinary differential equations with a known general solution. Next, the coefficients for the general solution were determined and the solution was written in terms of stress

giving equations 3.2.25-27. Next the Fourier transform was inverted to produce 3.2.28-30 in terms of stress.

After the rail only solution was presented, the same methods were used to solve the coating problem, which led to the system, 3.3.9, to solve. Next the finite difference method was introduced as a method to calculate the stresses when the shear modulus varied through the thickness of the coating. The finite difference approximation, 3.4.1, for the equations of motion and the boundary conditions, 3.4.3 and 3.4.6, were derived. Finally, the code was validated by comparison with the analytic solution in the transform domain. Then the number of partitions of the coating thickness, $n = 15$, for the finite difference method to converge to a minimum relative error of 10^{-4} was demonstrated.

Chapter 4. Results and Analysis

4.1 Introduction

This chapter investigates the nature of stress developed in the coating and the rail. First the problem with no coating is examined under the influence of several stress distributions in the spatial domain. A point source, a uniform distribution over the length of the shoe, and a parabolic distribution of stress are studied to understand how these distributions affect stress in the uncoated half-space. This is accomplished by using the analytic solution for the rail only problem.

The parabolic loading distribution is then used on the coated rail. Since the solution for the coated problem is numeric, a Fast Fourier Transform is used to invert the transform and study the results in the spatial domain for different constant shear moduli and various coating thickness. Then, using the finite difference code, the shear modulus is allowed to vary as a continuous function through the thickness of the coating. This continuous function allows the shear modulus to nearly vanish at the surface of the coating, simulating a liquid-like interface. It is also used to investigate a layered coating effect.

4.2 No Coating Results

4.2.1 Delta Distribution

For a point source, the force is applied to a single point on the surface of the rail, $\zeta = 0$, with the use of the Dirac delta function for the loading. The shear loading is introduced through the frictional effects. Thus, the shear load is taken to be a fraction of the direct load based on a coefficient of friction giving $\hat{f} = 0.2\delta(\zeta)$ and $\hat{k} = \delta(\zeta)$ in

equations 2.7.12 and 2.7.13. Equations 3.2.28, 3.2.29, and 3.2.30 are used to produce the following contour plots for the point source in the spatial domain.

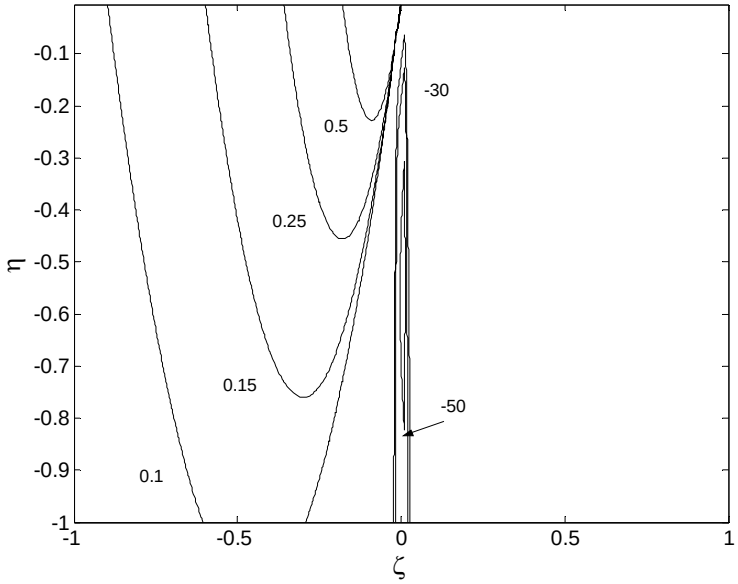

Figure 6. Point Source Direct Stress $\left(\sigma_{\zeta\zeta}\right)$ Contours

In Figure 6, the contours represent direct stress, $\sigma_{\zeta\zeta}$, in the direction of motion of the slipper. The horizontal axis is the direction of motion, ζ, with the positive to the right while the vertical axis is through the thickness of the rail, η, with the negative down. Even though the coating is not present, the no coating problem is still scaled relative to a coating thickness. The graph shows a width of one shoe length and a depth of one times the thickness of a coating assuming $\delta = h/l = 1.8x10^{-2}$. The labels on each contour are the relative magnitudes (recall stress is scaled by the shear modulus) of the stress for that curve. Notice in front of the source, the relative magnitudes of the stresses

are greater per depth into the rail than that of the stresses behind the source. Further the sign of the stress in front is negative while the sign is positive behind. This signifies the stress in front of the slipper is in compression while the stress behind the slipper is in tension. As ζ approaches zero, the magnitude of the stress becomes infinite because of the singularity at the origin. This is of course due to the singular nature of the loading function. Further as ζ moves away from the origin, the stress rates diminish rapidly. This is because the point source concentrates the applied force at the origin.

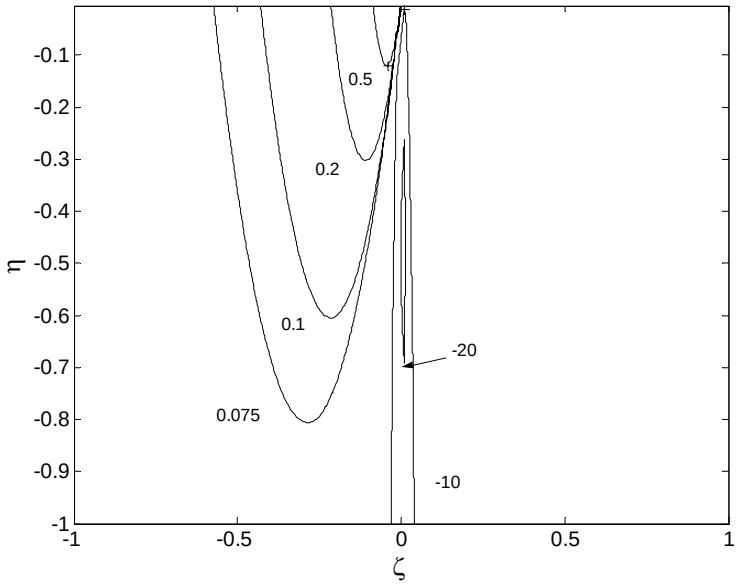

Figure 7. Point Source Direct Stress $\left(\sigma_{\eta\eta}\right)$ Contours

Figure 7 illustrates the direct stress, $\sigma_{\eta\eta}$, through the thickness of the rail in the spatial domain. The strength of the stress per depth is greater in front of the source just as with the stress in the direction of motion, $\sigma_{\zeta\zeta}$. The sign of the stress is negative in

front of the slipper showing a compression through the thickness of the rail. The sign is negative behind the slipper demonstrating tension. Just as with the direct stress in the direction of motion, the spike in the center signifies an increasing stress as ζ approaches zero due to the singular nature of the loading function.

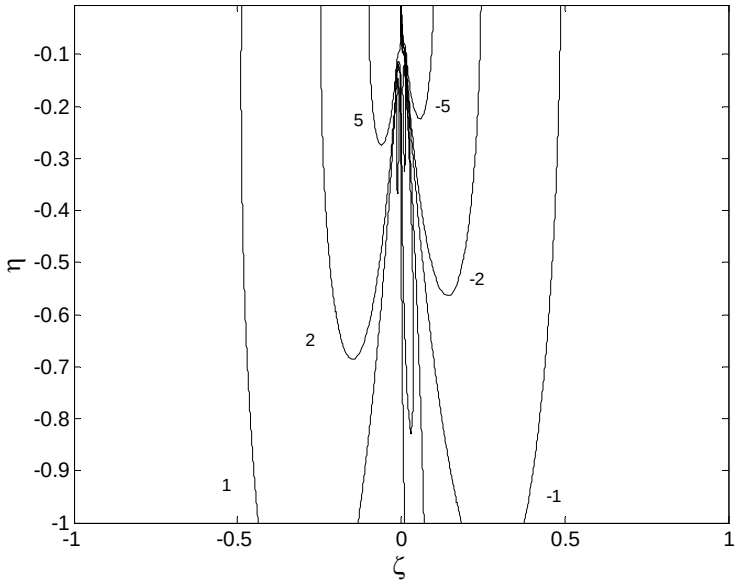

Figure 8. Point Source Shear Stress $\left(\tau_{\zeta\eta}\right)$ Contours

Figure 8 illustrates the shear stress, $\tau_{\zeta\eta}$, in the spatial domain. Notice the magnitudes of the shear stress per depth of penetration are significantly smaller than the direct stresses. This is because the shear loading was considered to be a fraction of the direct load. Additionally, the sign of the shear stress in front of the slipper is negative indicating the shear stress is in compression. At the same time, the sign of the stress

behind the slipper is positive indicating the direction of stress is in the direction of motion. Further, the unlabeled contours in the center of Figure 8 have the same magnitude with opposite signs as the contours from the top on the same side of the source. This is the behavior of the material in small neighborhood near $\zeta = 0$, which is directly beneath the point source. Just as with the direct stresses, the shear stress experiences the same singularity at the origin.

4.2.2 Uniform Distribution

With the uniform distribution, a constant load of magnitude one is applied to the entire length (0.2 meters) of the slipper so that $\hat{f} = 0.2H(1-|\zeta|)$ and $\hat{k} = H(1-|\zeta|)$.

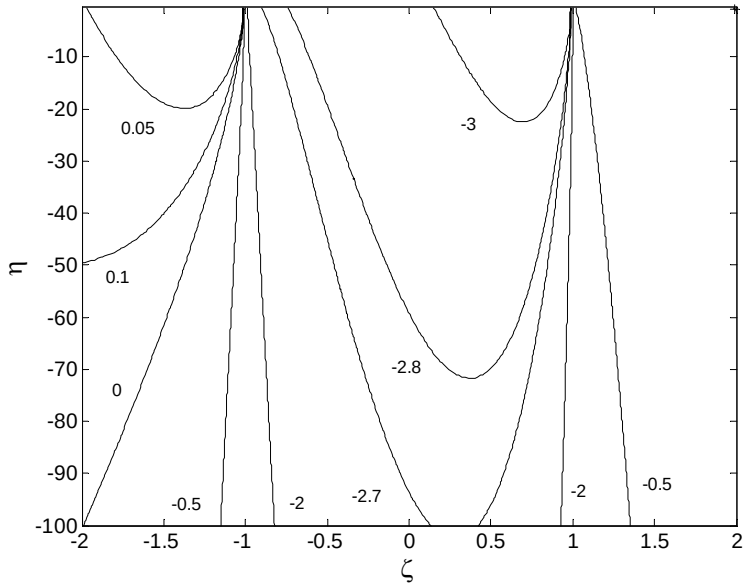

Figure 9. Uniform Source Direct Stress $\left(\sigma_{\zeta\zeta}\right)$ Contours

Figure 9 illustrates the behavior of the direct stress, $\sigma_{\zeta\zeta}$, in the direction of motion where ζ ranges over two times the length of the shoe and the depth, η, is 100

times the coating thickness. Since the uniform source is not as concentrated as the point source, it is necessary to look deeper into the rail to understand the behavior. The spreading of force from the uniform source enables the stress to distribute over more of the rail than the point source as well as limiting the penetration through the thickness. The value of the stress is negative from the back of the slipper, $\zeta = -1$, through the positive ζ axis. This implies the direct stress is in compression under and in front of the slipper. The stress changes sign at the rear of the slipper implying the stress is in tension behind the slipper. Also, notice that the magnitude of the stress is greatest propagating from beneath the slipper, $-1 < \zeta < 1$. Figure 10 illustrates the same behavior for the direct stress $\sigma_{\eta\eta}$ as $\sigma_{\zeta\zeta}$. Since the downward direction is the negative η axis, this also implies the stress is in compression beneath and in front of the slipper while the stress is in tension behind the slipper.

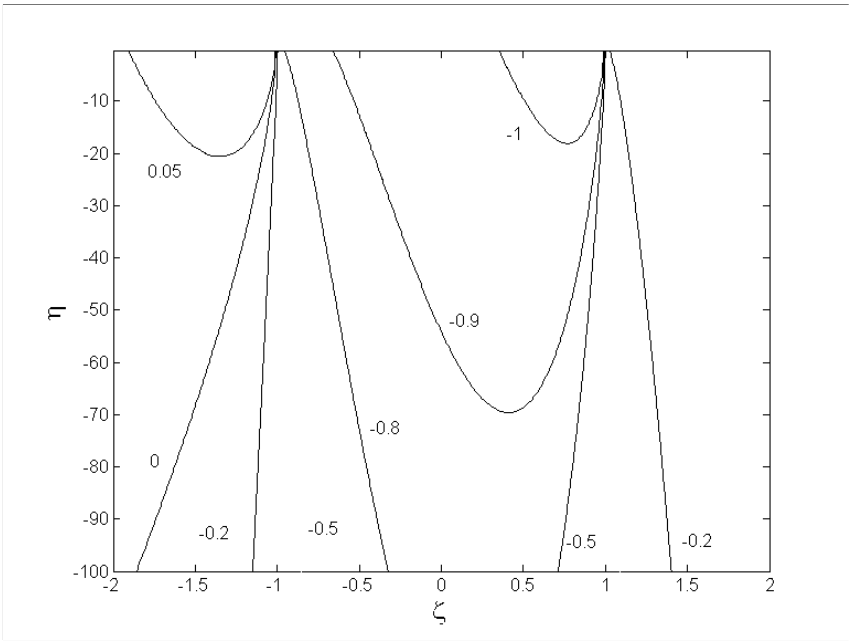

Figure 10. Uniform Source Direct Stress $\left(\sigma_{\eta\eta}\right)$ Contours

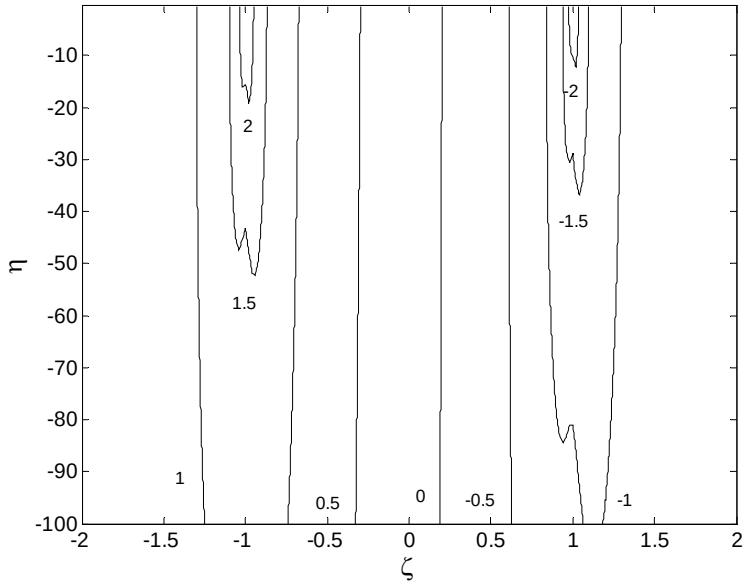

Figure 11. Uniform Source Shear Stress $\left(\tau_{\zeta\eta}\right)$ Contours

Figure 11 illustrates the shear stress, $\tau_{\zeta\eta}$, with a uniform source. Notice that if the load were not moving, the graph would be perfectly symmetric and the stress would be zero at the center of the slipper, $\zeta = 0$. Since the load is moving, the location of zero stress is shifted in the positive direction of motion. In front of the slipper, the sign of the stress values are negative indicating the shear stress is in compression. Behind the slipper, the sign is positive indicating the shear stress is in tension. Further, behind the slipper, the stresses of equal magnitudes as in front propagate further through the thickness, down the negative η axis.

4.2.3 Parabolic Distribution

With the parabolic distribution, the load is not constant over the length of the slipper. The load is greatest at the center of the slipper and weakest at the edges. Define the formula for the parabolic distribution as

$$f_L(x) = \begin{cases} \frac{3}{4L}(1-\frac{x^2}{L^2}) & |x| \le L \\ 0 & |x| > L \end{cases} \qquad 4.2.1$$

where L is the length of the slipper. The plots for the parabolic distribution use the value $L = 1$.

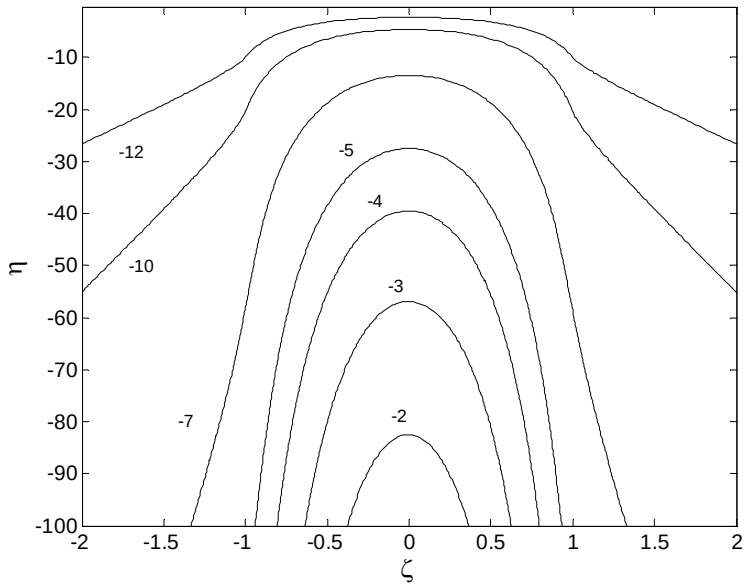

Figure 12. Parabolic Source Direct Stress $\left(\sigma_{\zeta\zeta}\right)$ Contours

Figure 12 illustrates the direct stress, $\sigma_{\zeta\zeta}$, in the direction of motion. All the magnitudes of stress are negative indicating the stress is in compression. Further, as ζ

and η approach zero, the curves are more concentrated. This is because the force due to loading is greatest in the center and the strength of the stress is weakening through the thickness. Figure 13 illustrates the direct stress, $\sigma_{\eta\eta}$, through the depth of the rail. The stress is of lower magnitude because it is primarily due to the direct stress loading function and does not reflect both boundary conditions like $\sigma_{\zeta\zeta}$, but has the same behavior as the stress in the direction of motion.

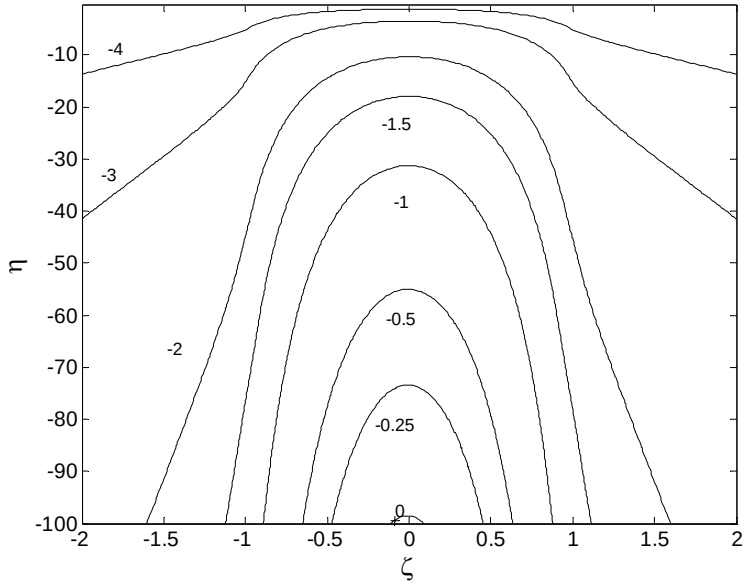

Figure 13. Parabolic Source Direct Stress $\left(\sigma_{\eta\eta}\right)$ Contours

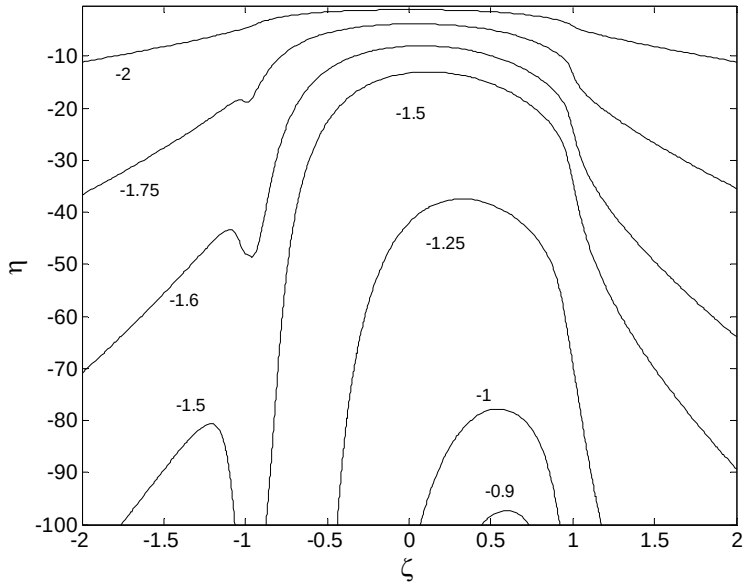

Figure 14. Parabolic Source Direct Stress $\left(\tau_{\zeta\eta}\right)$ Contours

Figure 14 illustrates the shear stress in the rail for the parabolic distribution. One interesting aspect of this graph is the similarities with the shear stress for the uniform source (Figure 11). Just like the uniform source, the motion shifts the graph to the right for the parabolic source. The value of the stress is negative indicating the stress is in compression.

The parabolic distribution is an interest in this study because the properties of this distribution can be easily observed in the problem with coating. When the coating is applied to the rail, it acts as a transfer function modifying the distribution of stress applied to the surface to a new distribution applied to the rail at $\eta = 0$. Before the coating problem is examined, first the properties of the parabolic distribution function are

examined. Notice from 4.2.1, that if $f_L(x)$ is stress, then $\int_{-L}^{L} f_L(x)dx$, or the area under the curve, is force. The area under this curve is always one despite the value for L, that is the total applied force is always one. The area denotes the strength of the applied load distributed over a region from $-L$ to L.

By increasing the value for L, the distribution of stress is applied to a larger surface without increasing the total applied force. This implies a weaker distribution of stress on the surface of the rail. Figure 15 illustrates the effects of increasing L. As L increases to 10, the stress of magnitude 1 is applied to the length from -10 to 10 rather than from -1 to 1 when $L = 1$.

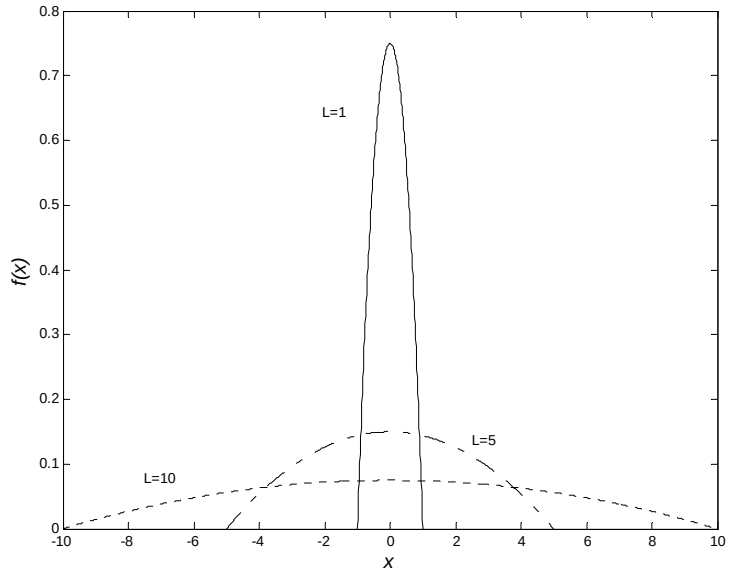

Figure 15. Comparison of the Parabolic Distribution Function with Different L values

This spreading effect in the stress applied to surface is the expectation for the coating acting as a transfer function.

4.3 Rail with Coating

This section investigates the effects on stress of coating the rail with a thin polymer or epoxy. First the effects of various thicknesses and shear moduli are studied. Then the distribution of stress is studied with the shear modulus varying as a function of thickness to investigate the effects of a vanishing shear modulus near the surface of the coating and layering coatings. The loading function used is the parabolic distribution with $L = 1$.

4.3.1 Effects of Coating Thickness and Shear Modulus

Recall that the coating thickness is reflected in the dimensionless parameter $\delta = h/l$, whose ranges are given in Table 3. The coating thickness is examined at three levels, $1.5x10^{-3}$ (low), $9.8x10^{-3}$ (mid), and $1.8x10^{-2}$ (high). The influence of the coating on the stress distribution in the rail will be depicted by the stress distribution at the interface, $\eta = 0$. Consequently, the graph of the parabolic distribution applied to the surface in the rail only problem is plotted with the stress curves for $\sigma_{\eta\eta}$ and $\tau_{\zeta\eta}$ to show the differences between the uncoated and coated problems. The parabolic distribution is not plotted with $\sigma_{\zeta\zeta}$ because the boundary conditions do not include direct stress in the direction of motion.

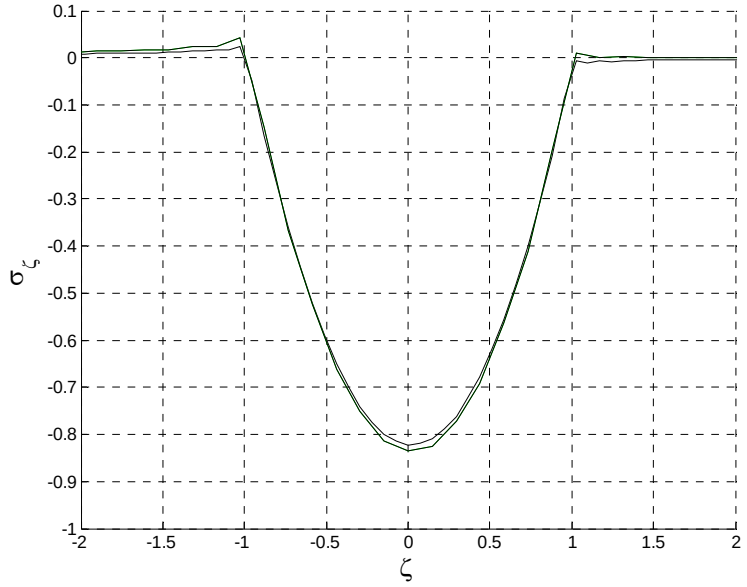

Figure 16. Comparison of Direct Stress $\left(\sigma_{\zeta\zeta}\right)$ with Respect to Coating Thickness

In Figure 16, the horizontal, ζ, axis is the direction of motion of the slipper and the vertical axis is the direct stress, $\sigma_{\zeta\zeta}$, in the direction of motion at $\eta = 0$. All stress generated comes from the two loading functions, $\hat{f}$ and $\hat{k}$. Even though the stress is plotted with respect to all three coating thicknesses; there is no distinct difference between them. Further, the load was applied from -1 to 1 on the ζ axis. All three curves also intersect the horizontal axis at $\zeta = -1$ and $\zeta = 1$ as does the load. This implies there is no difference in the spreading of the load between the three coating thicknesses.

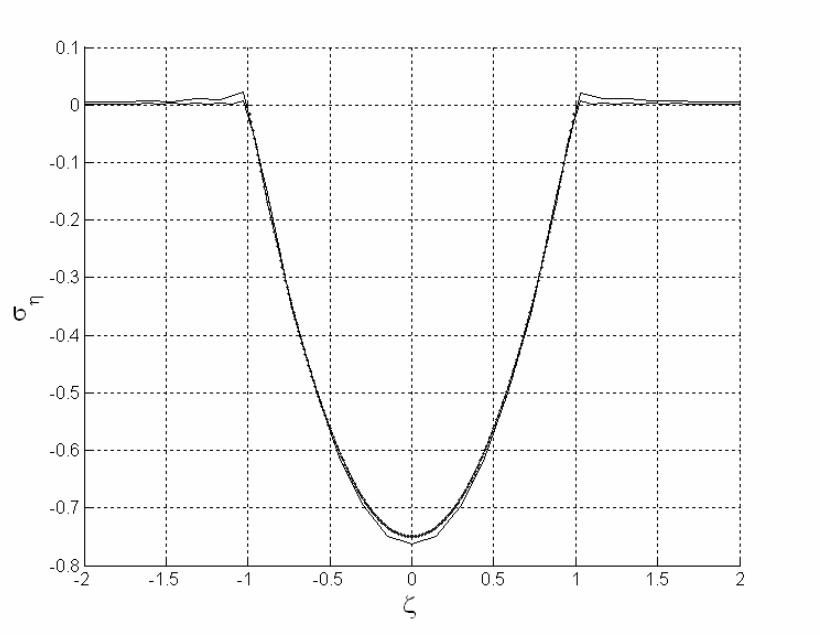

Figure 17. Comparison of Direct Stress $\left(\sigma_{\eta\eta}\right)$ with Respect to Coating Thickness

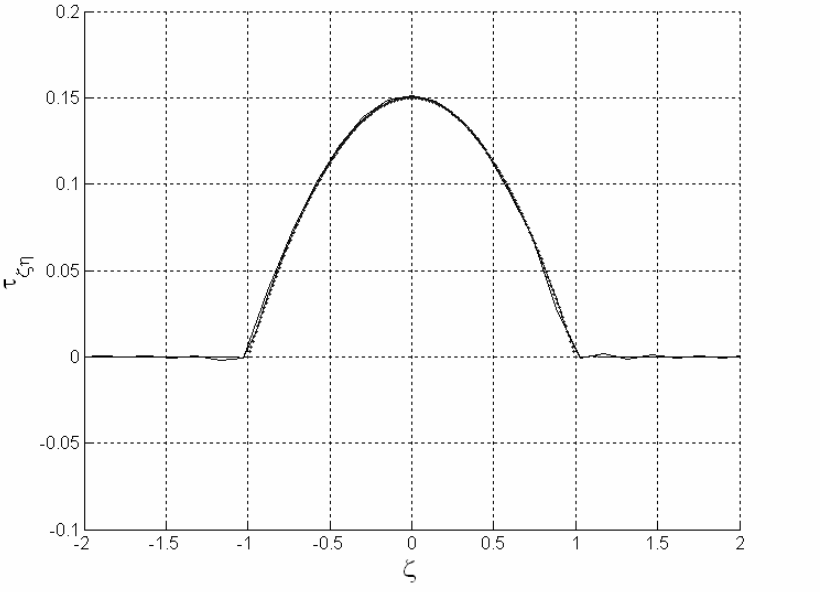

Figure 18. Comparison of Direct Stress $\left(\tau_{\zeta\eta}\right)$ with Respect to Coating Thickness

Figure 17 illustrates the effects of the coating thickness on direct stress, $\sigma_{\eta\eta}$, through the thickness. The load is graphed along with the stress. Figure 18 illustrates the effects of the coating thickness on shear stress, $\tau_{\zeta\eta}$. Notice in both figures, the peaks of the graphs do not show a significant difference, so the intensity or strength of the load has not changed due to the coating. Like the direct stress in the direction of motion, there is also no spreading effect due to the coating.

Next a constant shear modulus is varied to investigate its effect on the stress propagated into the rail. Recall the dimensionless parameter $G = G_2/G_1$ whose ranges are given in Table 3. This relationship implies that the dimensionless parameter G decreases as the shear modulus of the coating increases, so the three chosen parameters are 62 (low), 47 (mid), and 33 (high). In the following plots the parameter δ is always chosen as $1.5x10^{-3}$. The curves for $G = 33$ are the same curves as the $\delta = 1.5x10^{-3}$ in the figures for coating thickness.

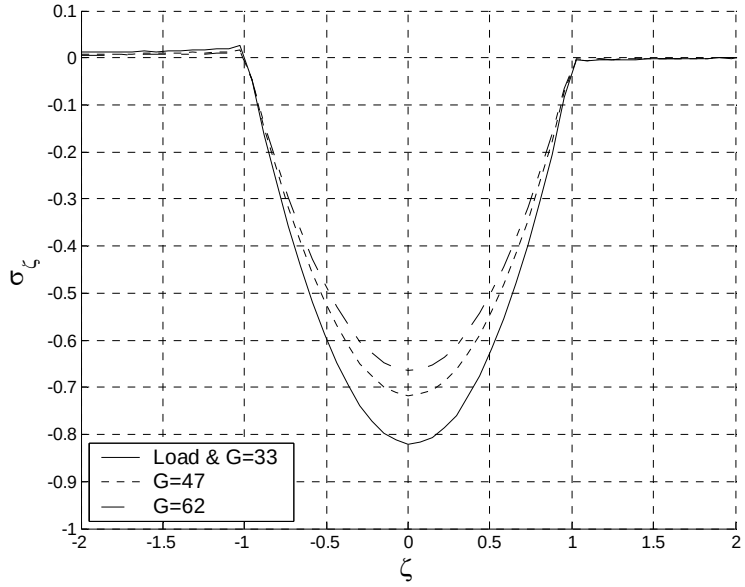

Figure 19. Comparison of Direct Stress $\left(\sigma_{\zeta\zeta}\right)$ with Respect to Shear Modulus

As illustrated in Figure 19, the direct stress, $\sigma_{\zeta\zeta}$, in the direction of motion is significantly affected in magnitude by the shear modulus of the coating. The area under the curve for $G = 33$ or the load is 1.09 while the area under the curve for $G = 62$ is 0.89. Recall, the area under the curve is the total application of force. This is an improvement of 0.2 in scaled force applied to the rail at the interface. As the dimensionless shear modulus decreases (increases in the coating), the strength of the stress at the interface between the rail and the coating increases. This implies that a lower shear modulus for the coating would allow less direct stress in the direction of motion at the interface with the rail. Because the load is not applied to the rail through the direct stress in the direction of motion, $\sigma_{\zeta\zeta}$, this does not imply that the stress distribution in the rail has been weakened. However, this reduction in stress can be

related to material yield or failure. Through theory on design stress or Von Mises stress, it can be shown that a reduction in the direct stress, $\sigma_{\zeta\zeta}$, can reduce the likelihood of material failure (20).

The figures for direct stress, $\sigma_{\eta\eta}$, through the thickness and shear stress, $\tau_{\zeta\eta}$, are not given separately because they are exactly the same as Figures 17 and 18, respectively. This demonstrates that the value of the shear modulus in the coating has very little effect on the direct stress through the thickness or the shear stress. It was expected that the higher shear modulus in the coating would disperse the load across a larger area of the rail due to the faster stress wave speed. However, the coating is too thin to see this effect.

If the shear modulus in the coating starts to approach zero, or become more liquid like, there is a greater effect in the direct stress in the direction of motion. Figure 20 illustrates this behavior with $G = 1000$, or $G_1 = 8x10^{-2}$ kg/ms^2, which is an unrealistic value for a polymer or epoxy adhesive.

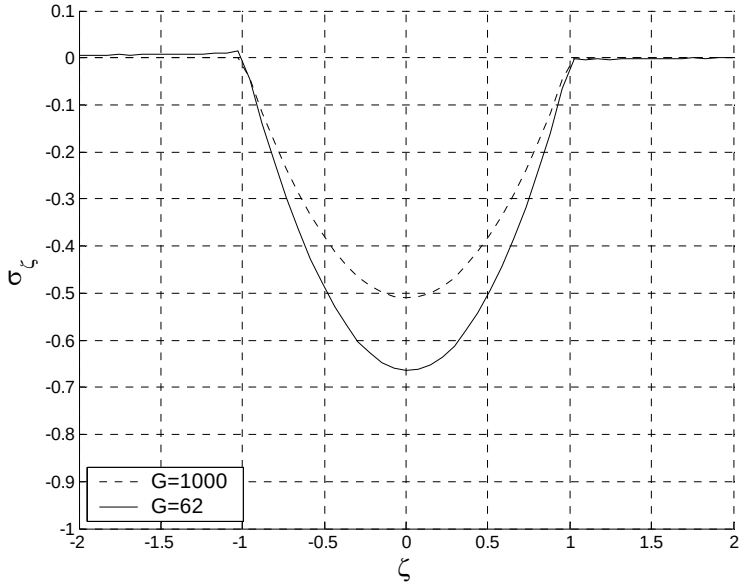

Figure 20. Comparison of Direct Stress $\left(\sigma_{\zeta\zeta}\right)$ with an Extremely Low Shear Modulus in the Coating

4.3.2 Variable Shear Modulus through the Thickness

This section investigates the affect varying the shear modulus as a function of thickness has on the stress distribution in the rail. The function $\hat{g}(\eta)$ in 2.8.1 and 2.8.2 is used to vary the shear modulus. A function similar is used for functionally graded materials (21:615). Define $\hat{g}(\eta)$ as

$$\hat{g}(\eta) = (G_t - G_b)\eta^m + G_b$$

where G_b is the starting shear modulus at the interface , G_t is the ending shear modulus at the surface of the coating, and *m* dictates the profile of variation through the thickness. Figure 21 illustrates the behavior of the function $\hat{g}(\eta)$ for different values of *m*. When *m*=1, the coating properties vary linearly through the thickness. When *m* is greater than

one, the material maintains a shear modulus close to its ending shear modulus through the thickness, and then the modulus vanishes close to the surface. When *m* is less than one, the materials shear modulus vanishes quickly as η approaches the surface of the coating.

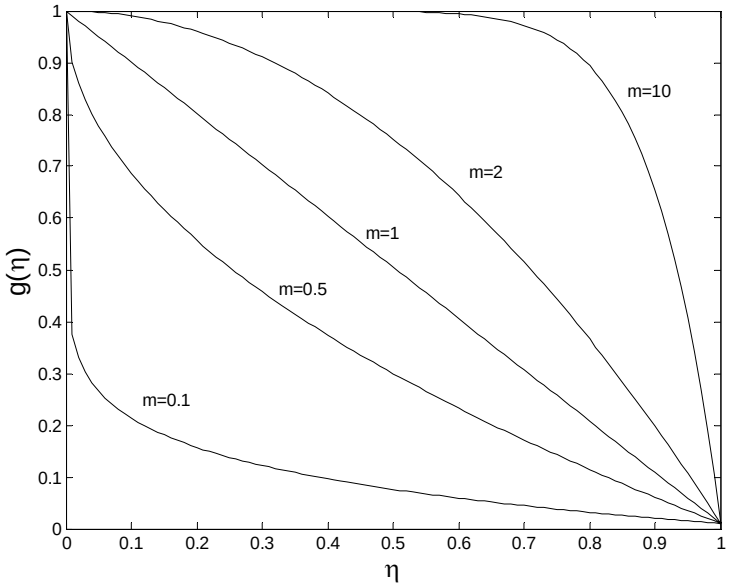

Figure 21. Behavior of Shear Modulus Varying Function $\hat{g}(\eta)$
For Different m Values

The graphs using the variable shear modulus function plotted for *m*=0.5 and *m*=2 are illustrated in Figures 22, 23, and 24. The best case for the constant shear modulus, $G = 62$, is also plotted for comparison. The input for $\hat{g}(\eta)$ is $G_t = 0.001$ and $G_b = 62$.

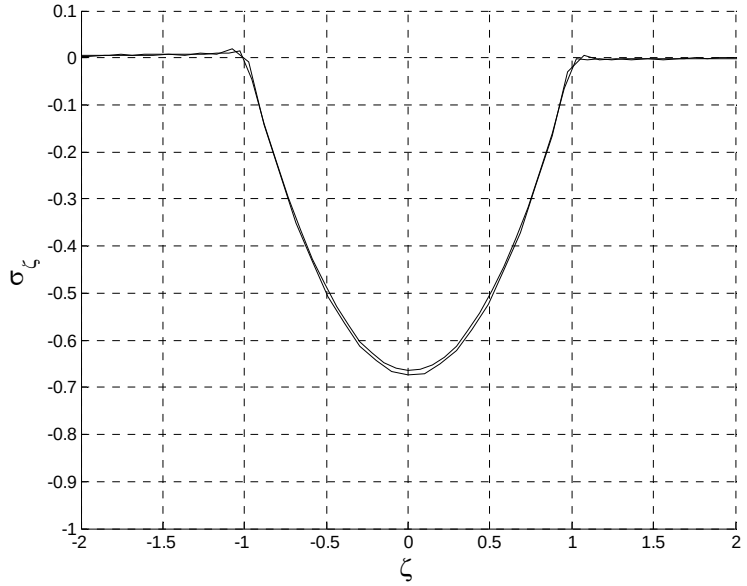

Figure 22. Comparison of Direct Stress $\left(\sigma_{\zeta\zeta}\right)$ for Variable Shear Modulus

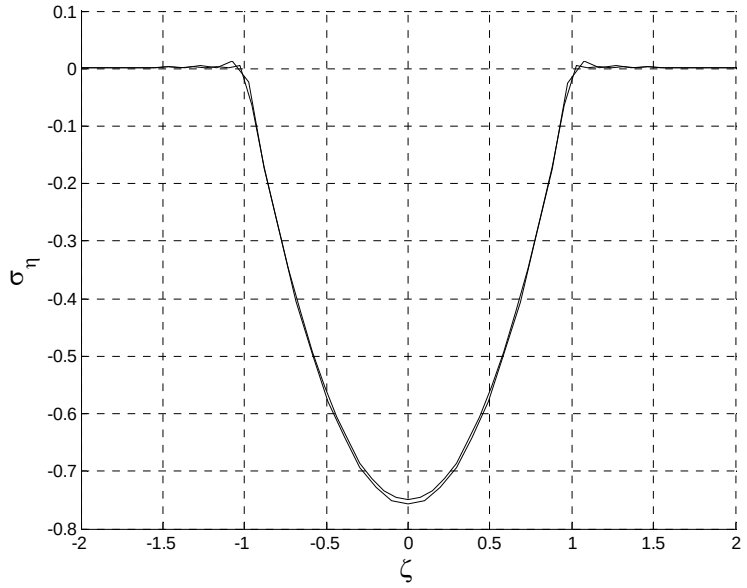

Figure 23. Comparison of Direct Stress $\left(\sigma_{\eta\eta}\right)$ for Variable Shear Modulus

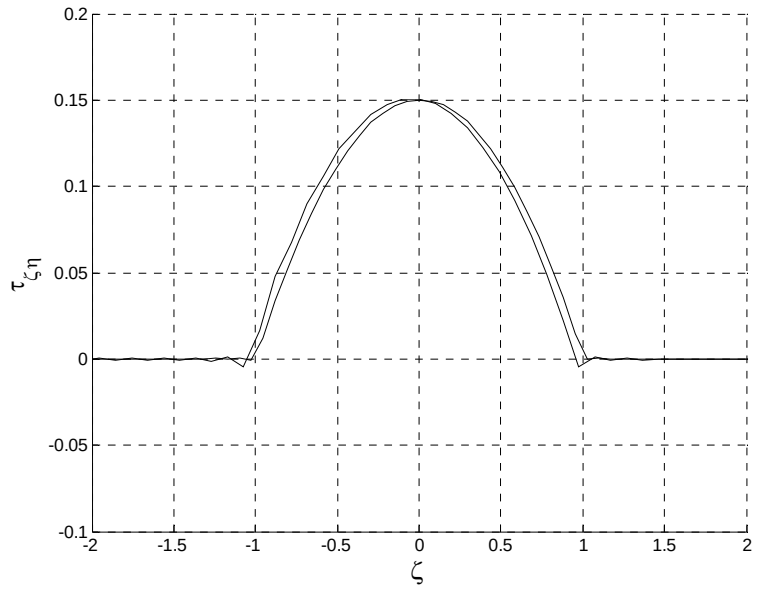

Figure 24. Comparison of Direct Stress $\left(\tau_{\zeta\eta}\right)$ for Variable Shear Modulus

In each figure, the curves are nearly indistinguishable. This illustrates there is no significant difference in layering coatings with different material properties versus having one material with a low shear modulus.

4.4 Summary

First the effects of the point source, uniform source, and parabolic source on stress distribution in the rail without coating were demonstrated. Then the effects of coatings on the parabolic stress distribution were studied. It was discovered that the presence of a thin coating, despite shear modulus or thickness, does not affect the spread of the distribution of force to the rail. Further, the thickness of the coating had little effect on the magnitude of the force propagating to the rail. Also, it was discovered that a lower shear modulus in the coating material produces a significantly lower direct stress

in the direction of motion. This does not imply a weaker load is transferred to the rail through the boundary conditions. However, it does imply that the probability of failure is reduced. This lower shear modulus implies the coating less rigid or stiff. Finally, it was shown that layering coatings produces no benefit greater than that of a constant shear modulus through the thickness of the coating.

Chapter 5. Summary and Conclusions

5.1 Summary

The first chapter of this thesis discussed the motivation for this research, the HHSTT's interest in mitigating the gouging phenomenon. Additionally, the chapter reviewed past research in half-space stress propagation and problem formulation, much of which was motivated by the transportation industry.

Next this thesis discussed the theory of interest to this study and the governing equations. The equations of motion 2.2.1-4 were stated along with the boundary and continuity condition to satisfy. The coordinate transformation was introduced and a detailed description of the dimension analysis was given. The equations of motion and the boundary and continuity conditions were transformed and scaled. Then the steady state system was introduced and given 2.8.1-4.

Chapter 3 described the methods used to solve the system and presented the solutions to the rail without coating problem as well as the coated rail problem. The Fourier transform was introduced for the rail only problem and an analytic solution was found in the transform domain by solving a homogeneous linear system of ordinary differential equations. The Fourier transform was inverted with respect to the stresses rather than the displacements. The solutions in the spatial domain for the no coating problem are given in 3.2.28-30. Then a similar method was used to solve the coated rail problem in the transform domain. Since the solutions were unsuitable for inverting the transform, a finite difference method was introduced yielding the difference model for the equations of motion 3.4.1 and the boundary conditions 3.4.3, 6. The chapter ended

with a point-wise comparison of the numerical method with the analytic solution in the transform domain to validate the code.

Chapter 4 began by illustrating the behavior of the material in the rail as stress propagated through the thickness of the steel with respect to a point source, a uniform source, and a parabolic source. Next, the parabolic loading function was used to examine the coating problem. Then the effects of various coating thicknesses and shear moduli were presented. Finally, the effect of layering coatings was also presented.

5.2 Significant Findings

The focus of this study was to understand how coating thickness and shear modulus affect the strength and distribution of stress in a half-space. This was motivated by a desire to mitigate the gouging phenomenon due to high speed impact loading. The coating thickness and shear modulus were limited by the realistic properties of the HHSTT. From Figures 16-18, it was deduced that the thickness of the coating in the ranges of interest had little to no affect on the strength or the distribution of the load to the rail. The lack of influence of this property is because the coating is likely too thin to see a significant effect on the stress

Even though the coating thickness had little effect, the shear modulus of the coating did have a significant effect on the direct stress, $\sigma_{\zeta\zeta}$, in the direction of motion. In Figures 19 and 20, as the dimensionless parameter, G , increases (shear modulus in the coating decreases), the strength of the stress is diminished. This implies coatings that are less stiff have a significant effect on the failure of the rail. Even though the gouging phenomenon was not present in the formulation of the problem, this is a significant factor

to consider when choosing coatings to mitigate gouging. The shear modulus does not have a significant effect on the distribution of the load over the surface of the rail.

It was also shown in Figures 22-24 that having a variable shear modulus through the thickness of the coating has no greater effect on the strength or distribution of stress than having a uniform coating with a low shear modulus. This implies that layering coatings of different material properties will not have a significant effect on stress distribution in the rail.

In summary, the strength of the force applied to the surface of the rail can be diminished by choosing a coating with a low shear modulus. The distribution of the stress over the surface of the rail will be virtually unaffected by the coating due to its thickness.

5.3 Suggestions for Future Study

This research investigated the problem as if the slipper had been traveling for an infinite amount of time. It also assumed the displacements in the rail and coating were not changing in the vicinity of the shoe with respect to time. It would be useful to see if the non-steady state problem behavior was drastically different from the steady state solution.

Even though the numerical results can determine certain behaviors, it would be of interest to have an analytic representation of the coated problem to understand mathematically why these behaviors exist. Even though the solutions in the Fourier domain are unsuitable for inverting the transform, approximation methods can be used to get an approximate analytic solution. Since the parameter δ is so small, it may be interesting to perform a perturbation and expand the system 3.3.9 in terms of δ. It is

expected that the leading order behavior of the analytic solution to the coated rail problem is the same or very similar to the solution to the no coating problem.

Appendix A: Q Matrix Derivation for Rail Only Problem

When finding the coefficients for the general solution to the rail only problem, the derivations became cumbersome and the matrix Q was introduced. From equation 3.2.22,

$$G\left\{\begin{bmatrix}1 & 0\\ 0 & q_2\end{bmatrix}\chi\begin{bmatrix}|\alpha|\,p_1 & 0\\ 0 & |\alpha|\,p_2\end{bmatrix}+\begin{bmatrix}0 & i\alpha\delta^2\\ i\alpha r_2 & 0\end{bmatrix}\chi\right\}\boldsymbol{\beta}=\begin{bmatrix}\delta F\\ -K\end{bmatrix}$$

Now, substituting 3.2.21 in for χ produces

$$G\left\{\begin{bmatrix}|\alpha|\,p_1 & |\alpha|\,p_2\\ i|\alpha|q_2\,\mathrm{sgn}(-\alpha) & i|\alpha|\dfrac{q_2p_2^2}{\delta^2}\mathrm{sgn}(-\alpha)\end{bmatrix}+\begin{bmatrix}-\alpha\dfrac{\delta^2}{p_1}\mathrm{sgn}(-\alpha) & -\alpha p_2\,\mathrm{sgn}(-\alpha)\\ i\alpha r_2 & i\alpha r_2\end{bmatrix}\right\}\boldsymbol{\beta}=\begin{bmatrix}\delta F\\ -K\end{bmatrix}$$

Since $|\alpha|\mathrm{sgn}(-\alpha)=-\alpha$ and $-\alpha\,\mathrm{sgn}(-\alpha)=|\alpha|$, divide the first row through by $|\alpha|$ and the second row through by $-i\alpha$. Also divide both sides by G and get

$$Q\boldsymbol{\beta}=\begin{bmatrix}\dfrac{\delta F}{|\alpha|G}\\ \dfrac{-iK}{\alpha G}\end{bmatrix}$$

where the matrix Q is defined as

$$Q=\begin{bmatrix}\dfrac{p_1^2+\delta^2}{p_1} & 2p_2\\ 1 & \dfrac{q_2p_2^2}{\delta^2}-r_2\end{bmatrix}$$

Appendix B: Convolutions with Loading Functions for Rail Only Solution

In 3.2.28-30 the solutions for stress are written in terms of convolutions with the applied loading functions. In chapter 4, these solutions are used to produce contour plots to determine the behavior of stress in the rail. In order to use these solutions the contours must be performed. Notice in 3.2.28-30, there are really only two term types to convolve with the loading functions because everything else is constant. They are

$$Z_i(\zeta,\eta)=\frac{\zeta}{p_i^2\eta^2+\zeta^2}$$

$$N_i(\zeta,\eta)=\frac{\eta}{p_i^2\eta^2+\zeta^2}$$

From chapter 4, the three loadings functions used are the Dirac delta function, the Heavyside function, and a parabolic function. First, notice that the convolution with the delta function is trivial, that is any function convolved with the delta function is just that function. The solutions in 3.2.28-30 are effectively the convolution with the delta function.

Next, the uniform distribution of force applied to the surface is accomplished through a constant times the Heavyside function, $H(1-|\zeta|)$. In this research, the constant load applied was one giving the convolutions as

$$\hat{f}*Z_i=\int_{-\infty}^{\infty}H(1-|\zeta|)\frac{\zeta-x}{(\zeta-x)^2+(p_i\eta)^2}dx$$

$$\hat{f}*N_i=\int_{-\infty}^{\infty}H(1-|\zeta|)\frac{\eta}{(\zeta-x)^2+(p_i\eta)^2}dx$$

Now the Heavyside function is zero outside the interval $-1<\zeta<1$ so the integrals reduce to

$$\hat{f} * Z_i = \int_{-1}^{1} \frac{\zeta - x}{(\zeta - x)^2 + (p_i\eta)^2} dx = \frac{1}{2} \ln \left| \frac{(\zeta+1)^2 + (p_i\eta)^2}{(\zeta-1)^2 + (p_i\eta)^2} \right|$$

$$\hat{f} * N_i = \int_{-1}^{1} \frac{\eta}{(\zeta - x)^2 + (p_i\eta)^2} dx = \frac{1}{p_i} \left[\tan^{-1}\left(\frac{\zeta+1}{p_i\eta} \right) - \tan^{-1}\left(\frac{\zeta-1}{p_i\eta} \right) \right]$$

Similarly, convolving the parabolic load, 4.2.1, with the solution gives

$$\hat{f} * Z_i = \frac{3}{4} \int_{-1}^{1} \frac{\zeta - x}{(\zeta - x)^2 + (p_i\eta)^2} \left(1 - (\zeta - x)^2\right) dx =$$
$$\frac{3}{8} \left[\ln \left| \frac{(\zeta+1)^2 + (p_i\eta)^2}{(\zeta-1)^2 + (p_i\eta)^2} \right| \left(1 - \zeta^2 + (p_i\eta)^2\right) + \right.$$
$$\left. 4 p_i \zeta \eta \left\{ \tan^{-1}\left(\frac{\zeta-1}{p_i\eta} \right) - \tan^{-1}\left(\frac{\zeta+1}{p_i\eta} \right) \right\} \right]$$

$$\hat{f} * N_i = \frac{3}{4} \int_{-1}^{1} \frac{\zeta - x}{(\zeta - x)^2 + (p_i\eta)^2} \left(1 - (\zeta - x)^2\right) dx =$$
$$\frac{1}{p_i} \left[\left\{ \tan^{-1}\left(\frac{\zeta-1}{p_i\eta} \right) - \tan^{-1}\left(\frac{\zeta+1}{p_i\eta} \right) \right\} \left(1 - \zeta^2 + (p_i\eta)^2\right) + \right.$$
$$\left. (\zeta+1) \ln \left| \left(\frac{\zeta+1}{p_i\eta} \right)^2 + 1 \right| - (\zeta-1) \ln \left| \left(\frac{\zeta-1}{p_i\eta} \right)^2 + 1 \right| - 2 \right]$$

Appendix C: Derivation of Boundary Conditions for Coating Problem

When finding the coefficients for the general solution to the coating problem system 3.3.9 was introduced. The matrix is comprised of sub blocks, R_1, R_2, L, found by using the loading condition 3.3.2 and the interface conditions 3.3.3 and 3.3.4. R_1 and R_2 are derived by applying 3.3.3 and 3.3.4 to the general solutions, 3.2.17, 3.2.18, 3.3.6, and 3.3.7. Using the interface condition 3.3.3 at $\eta = 0$ produces

$$\begin{bmatrix} 1 & 1 & 1 & 1 \\ x_1^{(2)} & x_2^{(2)} & x_3^{(2)} & x_4^{(2)} \end{bmatrix} \boldsymbol{A} = \begin{bmatrix} 1 & 1 \\ \dot{x}_1^{(2)} & \dot{x}_2^{(2)} \end{bmatrix} \boldsymbol{\beta}$$

where $\dot{x}$ symbolizes the eigenvectors associated with the rail (region II). Using the interface condition 3.3.4 at $\eta = 0$ produces

$$\begin{bmatrix} \lambda_1 + i\alpha\delta^2 x_1^{(2)} & \lambda_2 + i\alpha\delta^2 x_2^{(2)} & \lambda_3 + i\alpha\delta^2 x_3^{(2)} & \lambda_4 + i\alpha\delta^2 x_4^{(2)} \\ i\alpha r_1 + q_1\lambda_1 x_1^{(2)} & i\alpha r_1 + q_1\lambda_2 x_2^{(2)} & i\alpha r_1 + q_1\lambda_3 x_3^{(2)} & i\alpha r_1 + q_1\lambda_4 x_4^{(2)} \end{bmatrix} \boldsymbol{A} =$$
$$G \begin{bmatrix} |\alpha| \left(\frac{p_1^2 + \delta^2}{p_1} \right) & 2|\alpha| p_2 \\ -i\alpha & i\alpha \left(r_2 - \frac{q_2 p_2^2}{\delta^2} \right) \end{bmatrix} \boldsymbol{\beta}$$

Combining the two interface conditions together produces the system

$$\begin{bmatrix} R_1 & R_2 \end{bmatrix} \begin{bmatrix} \boldsymbol{A} \\ \boldsymbol{\beta} \end{bmatrix} = \begin{bmatrix} \boldsymbol{0} \end{bmatrix}$$

where

$$R_1 = \begin{bmatrix} 1 & 1 & 1 & 1 \\ x_1^{(2)} & x_2^{(2)} & x_3^{(2)} & x_4^{(2)} \\ \lambda_1 + i\alpha\delta^2 x_1^{(2)} & \lambda_2 + i\alpha\delta^2 x_2^{(2)} & \lambda_3 + i\alpha\delta^2 x_3^{(2)} & \lambda_4 + i\alpha\delta^2 x_4^{(2)} \\ i\alpha r_1 + q_1\lambda_1 x_1^{(2)} & i\alpha r_1 + q_1\lambda_2 x_2^{(2)} & i\alpha r_1 + q_1\lambda_3 x_3^{(2)} & i\alpha r_1 + q_1\lambda_4 x_4^{(2)} \end{bmatrix}$$

$$R_2 = \begin{bmatrix} -1 & -1 \\ -\dot{x}_1^{(2)} & -\dot{x}_2^{(2)} \\ -G|\alpha|\left(\frac{p_1^2 + \delta^2}{p_1}\right) & -2G|\alpha|\, p_2 \\ i\alpha G & -i\alpha G\left(r_2 - \frac{q_2 p_2^2}{\delta^2}\right) \end{bmatrix}$$

Now L is derived by applying 3.3.2, at $\eta = 1$, to the general solutions to produce

$$\begin{bmatrix} e^{\lambda_1}\left(\lambda_1 + i\alpha\delta^2 x_1^{(2)}\right) & e^{\lambda_2}\left(\lambda_2 + i\alpha\delta^2 x_2^{(2)}\right) & e^{\lambda_3}\left(\lambda_3 + i\alpha\delta^2 x_3^{(2)}\right) & e^{\lambda_4}\left(\lambda_4 + i\alpha\delta^2 x_4^{(2)}\right) \\ e^{\lambda_1}\left(i\alpha r_1 + q_1\lambda_1 x_1^{(2)}\right) & e^{\lambda_2}\left(i\alpha r_1 + q_1\lambda_2 x_2^{(2)}\right) & e^{\lambda_3}\left(i\alpha r_1 + q_1\lambda_3 x_3^{(2)}\right) & e^{\lambda_4}\left(i\alpha r_1 + q_1\lambda_4 x_4^{(2)}\right) \end{bmatrix} \boldsymbol{A} = \begin{bmatrix} \delta F \\ -K \end{bmatrix}$$

So let L be the 2x4 matrix on the left hand side of the equation and combine with the results from above to produce 3.3.9:

$$\begin{bmatrix} R_1 & R_2 \\ L & 0_{2x2} \end{bmatrix} \begin{bmatrix} \boldsymbol{A} \\ \boldsymbol{\beta} \end{bmatrix} = \begin{bmatrix} \boldsymbol{0} \\ \boldsymbol{F} \end{bmatrix}$$

Appendix D: Derivation of Boundary Condition Matrices for the Numerical Method

Equation 3.4.5 gave the form of the boundary condition at $\eta = 0$ where $\boldsymbol{H}$ captures the influence of the rail on the coating. Recall, $\boldsymbol{H}$ is found by substituting 3.4.4 for $\boldsymbol{\beta}$ in the left hand side of 3.2.22 and substituting into 3.3.4. This produces the following results:

$$\boldsymbol{H} = \begin{bmatrix} 0 & i\alpha\delta^2 \\ i\alpha\delta^2 & 0 \end{bmatrix} - G\begin{bmatrix} 1 & 0 \\ 0 & q_2 \end{bmatrix}\chi\begin{bmatrix} |\alpha| p_1 & 0 \\ 0 & |\alpha| p_2 \end{bmatrix}\chi^{-1} - G\begin{bmatrix} 0 & i\alpha\delta^2 \\ i\alpha r_2 & 0 \end{bmatrix}$$

which with some simplification yields

$$\boldsymbol{H} = \begin{bmatrix} 0 & i\alpha\delta^2(1-G) \\ i\alpha\left(\delta^2 - Gr_2\right) & 0 \end{bmatrix} - G\begin{bmatrix} 1 & 0 \\ 0 & q_2 \end{bmatrix}\chi\begin{bmatrix} |\alpha| p_1 & 0 \\ 0 & |\alpha| p_2 \end{bmatrix}\chi^{-1}$$

Next, the difference equation was given for the boundary condition which produced a ghost point. This boundary condition was then substituted into 3.4.1 to give 3.4.6 where the matrix $\hat{G}$ is

$$\hat{G} = \begin{bmatrix} a_0h^2 + 2 & 0 \\ 0 & c_0h^2 + 4q_1 \end{bmatrix} - 2h\begin{bmatrix} 1 & \dfrac{-b_1h}{2} \\ \dfrac{-b_2hq_2}{2q_1} & 2q_2 \end{bmatrix}\begin{bmatrix} 1 & 0 \\ 0 & \dfrac{1}{q_1} \end{bmatrix}\boldsymbol{H}$$

References

1. Szmerekovsky, Andrew G. *The Physical Understanding of the Use of Coatings to Mitigate Hypervelocity Gouging Considering Real Test Sled Dimensions.* Air Force Institute of Technology (AU), Wright-Patterson AFB OH, September 2004 (ADA427344).

2. Sun, Lu. "Dynamic Displacement Response of Beam-type Structures to Moving Line Loads," *International Journal of Solids and Structures*, 38:8869-8878 (2001).

3. Sun, Lu. "A Closed-form Solution of a Bernoulli-Euler Beam on a Viscoelastic Foundation Under Harmonic Line Loads," *Journal of Sound and Vibration*, 242:619-627 (2001).

4. Lee, H.P. "Dynamimc Response of a Beam With a Moving Mass," *Journal of Sound and Vibration*, 191: 289-294 (1996).

5. Rao, Visweswara. "Linear Dynamics of an Elastic Beam Under Moving Loads," *Journal of Vibration and Acoustics*, 122: 281-289 (July 2000).

6. Gbadeyan J.A. and S.T. Oni. "Dynamic Behaviour of Beams and Rectangular Plates Under Moving Loads," *Journal of Sound and Vibration*, 182: 677-695 (May 1995).

7. Choros, J. and G.G. Adams. "A Steadily Moving Load on an Elastic Beam Resting on a Tensionless Winkler Foundation," *Journal of Applied Mechanics*, 46: 175-179 (March 1979).

8. Soldatenkov, I.A. "Approximate Solution of the Wear Problem for a Thin Strip Connected to an Elastic Half-Plane," *Mechanics of Solids*, 32(1): 38-44 (1997).

9. Aleksandrov, V.M. and N.Kh. Arutiunian. "Interaction of a Moving Elastic Stamp With an Elastic Half-Plane Through a Stiffener or a Thin Ideal Fluid Layer," *Prikladnaya Matematika i Mekhanika (PMM)*, 42(3): 475-485 (1978).

10. de Barros, F.C.P. and J.E. Luco. "Response of a Layered Viscoelastic Half-Space to a Moving Point Load," *Wave Motion*, 19:189-210 (1994).

11. Kennedy, T.C. and G. Herrmann. "Moving Load on a Fluid-Solid Interface: Supersonic Regime," *Journal of Applied Mechanics*, 137-142 (March 1973).

12. Vigak, V.M. "Correct Solutions of Plane Elastic Problems for a Half-Plane," *International Applied Mechanics*, 40: 283-289 (2004).

13. Dieterman, H.A. and A. Metrikine. "Critical Velocities of a Harmonic Load Moving Along an Elastic Layer," *Journal of Applied Mechanics*, 64: 596-600 (September 1997).

14. Dal', Yu M. "On the Point Force at the Boundary of the Elastic Half-Plane," *Physics-Doklady*, 39(9): 645-646 (September 1994).

15. Hu, Caifeng and G.A. Hartley. "Analysis of a Thin Plate on an Elastic Half-Space," *Computers and Structures*, 52(2): 227-235 (1994).

16. Verruijt, A. and C. Cornejo Cordova. "Moving Loads on an Elastic Half-Plane with Hysteretic Damping," *Journal of Applied Mechanics*, 68: 915-922 (November 2001).

17. Fung, Y.C. *Foundation of Solid Mechanics*. New Jersey: Prentice-Hall, 1965.

18. Timenshenko, S.P. and J.N. Goodier. *Theory of Elasticity*. New York: McGraw-Hill Company, 1970.

19. Lin, C.C. and L.A. Segel. *Mathematics Applied to Deterministic Problems in Natural Sciences*. Society for Industrial and Applied Mathematics, 1988.

20. "Strength of Materials." Exerpt from unpublished article. n. pag. http://www.engineersedge.com/strength_of_materials.htm. Engineers Edge. 15 February 2005.

21. Reddy, J.N. *Mechanics of Laminated Composite Plates and Shells: Theory and Analysis.* New York: CRC Press, 2003.

REPORT DOCUMENTATION PAGE

Form Approved
OMB No. 074-0188

1. REPORT DATE *(DD-MM-YYYY)*	**2. REPORT TYPE**	**3. DATES COVERED** *(From – To)*
21-03-2005	Master's Thesis	August 2003 – March 2005

4. TITLE AND SUBTITLE

Steady State Stress in a Coated Infinite Half-Space Subjected to a Moving Load

5a. CONTRACT NUMBER

5b. GRANT NUMBER

5c. PROGRAM ELEMENT NUMBER

6. AUTHOR(S)

Cruthirds, Jason M., First Lieutenant, USAF

5d. PROJECT NUMBER

5e. TASK NUMBER

5f. WORK UNIT NUMBER

7. PERFORMING ORGANIZATION NAMES(S) AND ADDRESS(S)
Air Force Institute of Technology
Graduate School of Engineering and Management (AFIT/EN)
2950 Hobson Way, Building 640
WPAFB OH 45433-8865

8. PERFORMING ORGANIZATION REPORT NUMBER

AFIT/GCCS/ENC/05-01

9. SPONSORING/MONITORING AGENCY NAME(S) AND ADDRESS(ES)
Air Force Office of Scientific Research
Attn: Dr. Neal D. Glassman
4015 Wilson Blvd. Room 713
Arlington VA 22203-1954

10. SPONSOR/MONITOR'S ACRONYM(S)
AFOSR/NM

11. SPONSOR/MONITOR'S REPORT NUMBER(S)

12. DISTRIBUTION/AVAILABILITY STATEMENT

APPROVED FOR PUBLIC RELEASE; DISTRIBUTION UNLIMITED.

13. SUPPLEMENTARY NOTES

14. ABSTRACT

This research investigates the use of coatings to mitigate the stress distribution into an infinite half-space. High energy impact phenomenon at velocities exceeding the speed of sound is an important area of interest to the Air Force Research Laboratory. Holloman Air Force Base's High Speed Test Track sustains significant damage due to this phenomenon. In this thesis, the track system and coating are modeled analytically with equations of motion in terms of linear displacements. Coating thickness and material properties of epoxy or polymer laminates are investigated to understand their affect of stress distribution in the rail. An analytic solution is used to verify a finite difference method. It is found that due to limitations in coating thickness of the track system, this property has no significant affect on the stress distribution. However, the shear modulus of the material is found to have a significant affect representing the possible onset of material failure through the consideration of the combined stress field at the coating-rail interface.

15. SUBJECT TERMS

Half-space, coatings, stress

16. SECURITY CLASSIFICATION OF:			**17. LIMITATION OF ABSTRACT**	**18. NUMBER OF PAGES**	**19a. NAME OF RESPONSIBLE PERSON**
a. REPORT	**b. ABSTRACT**	**c. THIS PAGE**			William P. Baker, Ph.D. (AFIT/ENC)
U	**U**	**U**	**UU**	92	**19b. TELEPHONE NUMBER** *(Include area code)* (937) 255-3636, ext 4517 (William.Baker@afit.edu)

Standard Form 298 (Rev. 8-98)
Prescribed by ANSI Std. Z39-18